NOVEL $Bi_4NbO_8Cl/g\text{-}C_3N_4$ NANOCOMPOSITE FOR IMPROVED PHOTOCATALYTIC DEGRADATION OF METHYLENE BLUE DYE UNDER VISIBLE LED LIGHT ILLUMINATION

Thesis Submitted
By

Mahabub Rahaman Laskar
Class Roll No.- 002210402024
Examination Roll No.- M4CIV24021
Registration No.- 163471 of 2022-2023

MASTER OF ENGINEERING

Under the supervision of

Prof. Ankush Majumdar

DEPARTMENT OF CIVIL ENGINEERING
(ENVIRONMENTAL ENGINEERING DIVISION)
JADAVPUR UNIVERSITY
KOLKATA-700 032, INDIA
2024

Declaration

*The Thesis titled "**Novel $Bi_4NbO_8Cl/g\text{-}C_3N_4$ nanocomposite for improved photocatalytic degradation of methylene blue dye under visible LED light illumination**" is prepared and submitted for the award of the degree of **Master of Engineering in Civil Engineering** course of **Jadavpur University** for the session of 2022-2024. I hereby declare that all of the work included in this thesis is original to me. The work mentioned in this thesis has not been submitted in part to support an application for a different degree or certificate from this university or any other. All sources of information or assistance used in the thesis have been properly credited.*

Mahabub Rahaman Laskar

Mahabub Rahaman Laskar
M.C.E- 2ND Year
Class Roll No.- 002210402024
Examination Roll No.- M4CIV24021
Registration No.- 163471 of 2022-2023
Department of Civil Engineering
Environmental Engineering Division
Jadavpur University

Date: 31/05/2024

JADAVPUR UNIVERSITY
DEPARTMENT OF CIVIL ENGINEERING
KOLKATA-700 032

Recommendation Certificate

*This is to certify that the thesis entitled "**Novel Bi_4NbO_8Cl/g-C_3N_4 nanocomposite for improved photocatalytic degradation of methylene blue dye under visible LED light illumination**" is prepared and submitted by Mahabub Rahaman Laskar, be accepted in partial fulfilment of the requirements for the Degree of Master of Civil Engineering with specialization Environmental Engineering from Jadavpur University is absolutely based upon his own work under the super vision of **Prof. Ankush Majumdar** and that neither his thesis nor any part of this thesis has been submitted for any degree or any other academic award anywhere before.*

Signature of the supervisor and date with office seal

30/05/24

Ankush Majumdar
Assistant Professor
Department of Civil Engineering
Jadavpur University

Countersigned by

Assistant Professor
Department of Civil Engineering
Jadavpur University
Kolkata-700 032

Dipak Laha 31/5/24

Dean
Faculty of Engineering Technology
Jadavpur University

DEAN
Faculty of Engineering & Technology
JADAVPUR UNIVERSITY
KOLKATA-700 0

for HOD Bhattacharjee 31/5/24

Head of Department
Department of Civil Engineering
Jadavpur University

Head
Department of Civil Engineering
Jadavpur University
Kolkata-700 032

JADAVPUR UNIVERSITY
DEPARTMENT OF CIVIL ENGINEERING
KOLKATA-700 032

CERTIFICATE OF APPROVAL

This certifies that the thesis has been accepted as an original work completed and presented in a way that justifies acceptance as a requirement for the degree for which it has been submitted. The undersigned acknowledges that by granting this approval, they do not necessarily support or agree with any assertions made, viewpoints expressed, or conclusions reached in the thesis; rather, they simply authorise it for the intended use.

Final examination for evaluation of thesis

1. ----------

2. ----------

3. ----------

4. ----------

Acknowledgement

I am extremely thankful and indebted to Prof. Ankush Majumdar, Assistant Professor of Civil Engineering Department, Jadavpur University, for his valuable guidance, constant support and encouragement throughout my thesis work. This thesis would never been completed without his blessings, guidance. Constant vigil, careful supervision and inspiration throughout the session.

I am sincerely thankful and obliged to other professors of Environmental Engineering Division Prof. S. Chakraborty, Prof. S.N. Mukherjee, Prof. T. Hazra, Prof. Anupam Deb Sarkar, Prof. A. Dutta, Prof. A. Roy for their constant and thorough guidance during my coursework of Master of Civil Engineering lead me the acquiring of clear concept of Environmental Engineering help me to understand the subject of thesis work as well full completion and submission within stipulated period.

Last but not the least, I express my sincere gratitude to all of my batch mates of Environmental Engineering Division for being with me.

Mahabub Rahaman Laskar

Place: Kolkata
Date: 31/05/2024

Mahabub Rahaman Laskar
M.C.E- 2ND Year
Class Roll No.- 002210402024
Examination Roll No.- M4CIV24021
Registration No.- 163471 of 2022-2023
Department of Civil Engineering
Environmental Engineering Division
Jadavpur University

ABSTRACT

A novel visible-light-responsive Bi_4NbO_8Cl/g-C_3N_4 nanocomposite photocatalyst was hydrothermally produced using Bi_4NbO_8Cl and g-C_3N_4. Methylene Blue'(MB) deterioration under visible LED light is an emergent dye pollution. The photocatalytic efficiency of the nanocomposite materials was evaluated using irradiation. At an ideal mass ratio of 1:2 (50mg of Bi_4NbO_8Cl to 100 mg of g-C_3N_4), the 50-Bi_4NbO_8Cl/g-C_3N_4 (50-BNOC/UGCN) nanocomposite was found to have the best photocatalytic degradation efficiency toward MB. The photocatalytic degradation of MB (10 mg/l) by 50-Bi_4NbO_8Cl/g-C_3N_4 (1 g/l) during 60 minutes of visible 20W LED light irradiation was 99.35%. The development of Z-scheme heterojunctions, which led to reduced recombination of photogenerated electron-hole pairs and improved visible light absorption, was responsible for this enhanced performance. The results not only demonstrate the construction of the Bi_4NbO_8Cl/g-C_3N_4 nanocomposite for the successful degradation of resistant pollutants by photocatalysis at affordable prices and energy efficiency, but they also promote the development of related photocatalysts aimed for environmental remediation.

CONTENTS

List of Tables

Page No.

List of Figures

Page No.

LIST OF ABBREVATION

AOP	Advance Oxidation Process
BMO	Bismuth molybdenum oxide
BOD	Biochemical Oxygen Demand
BQ	Benzoquinone
CB	Conduction Band
COD	Chemical Oxygen Demand
CR	Congo Red
EDTA	Ethylenediamine tetraacetic acid
IPA	Isopropanol
KHP	Potassium Hydrogen Pthalate
LED	Light Emitting Diode
MB	Methylene Blue
MG	Methyl Green
MO	Methyl Orange
NF	Nano Filtration
RhB	Rhodamine B
RO	Reverse Osmosis
ROS	Reactive Oxygen Species
VB	Valance Band

CHAPTER 1

1.1 INTRODUCTION

Methylene blue (MB) is noteworthy in history since it was the first synthetic substance and antiseptic colour to be used therapeutically in clinical medicine. Prior to the development of penicillin and sulfonamides, MB and its derivatives were frequently used in chemotherapy. Additionally, MB has been a lead molecule in medication development against cancer and a variety of viral and bacterial illnesses. Methylene blue is a dye that works well in a lot of different sectors. It has a great affinity for cotton, wool, and silk fibres, which makes it a popular dye in the textile industry. It produces a brilliant, stable blue hue that is resistant to fading. Due of its affordability, it is a well-liked option for producing fabrics on a wide scale.
For staining and biochemical experiments, it is essential in biological and laboratory contexts. In terms of medicine, it has antibacterial qualities, serves as an antidote for several poisonings, and is an essential treatment for methemoglobinemia. It is also crucial for treating fish diseases and keeping an eye on water quality in aquaculture. MB is an organic chloride salt that has a bright greenish appearance and this dye's colour in solution is blue. It is also referred to as methylthioninium chloride. It's categorised as a phenothiazine, more precisely as a diamino phenothiazine. Its molecular weight is 319.85 g/mol and its chemical formula is $C_{16}H_{18}N_3Sl$ (Oladoye et al., 2022).

Every year, hundreds of tonnes of these dyes are generated in large quantities all over the world (M. Chen et al., 2021). To be precise, the industrial production of dye compounds is around 7×10^5 tonnes per year (Katheresan et al., 2018). Aniline blue, alcian blue, basic fuchsin, methylene blue, crystal violet, toluidine blue, and congo red are a few instances of synthetic dyes. According to a report, the textile industry accounts for almost 67% of the dyestuff market and/or consumption, and for every tonne of fibre produced, about 120 cubic metres of industrial wastewater are released (J. Zhang et al., 2009). Furthermore, aquatic life, beneficial bacteria, human lives, and health have all been put in danger as a result of the careless discharge of industrial wastewater into natural water sources, which has been noted to be a common disposal pathway. This is due to the fact that dyes like MB have been discovered to be significantly hazardous at high concentrations (Hameed et al., 2007). The molecular structure of MB, has an aromatic ring that is characteristically stable and renders the substance non-biodegradable and carcinogenic (Hassaan et al., 2017). The health hazards linked to coming into contact with MB include, but are not limited to, respiratory disorders, gastrointestinal troubles, cardiovascular problems, genitourinary

complications, and dermatological impacts (Hassani et al., 2008). The dyes are challenging to cure by biotreatment because of their complex molecular architectures. Due to the non-biodegradable nature of dyes, textile waste water frequently has low BOD to COD ratios (Katheresan et al., 2018).

In order to avoid the harmful consequences that MB poses to the environment and human health, its removal from effluent wastes is crucial (Thabede et al., 2020). The application of MB in healthcare can be managed in relation to regulating the recommended dosage. Hence, wastewater and effluents from industries are the primary target of the removal procedures. Before being released into the environment, MB can be removed from its waste and effluent elements using a variety of technologies that have been proposed and established. According to Dutta et al. (Dutta et al., 2011), effective removal strategies available today can be generally categorized as physical, chemical, or biological processes. This suggests that the three techniques listed are traditional and have undergone thorough investigation by scientists and/or environmentalists. More sub-separation techniques that have been suggested for the removal of MB from sewage and wastewater include oxidation, photocatalyzed degradation, biodegradation, biocatalytic degradation, and adsorption processes (Oladoye et al., 2022). Additional methods include microwave treatment, liquid-liquid extraction, ultrafiltration, nanofiltration, vacuum membrane distillation, and phytoremediation (Stephenson @ & Dufft, 1996). Studies have revealed, nevertheless, that the majority of these conventional techniques have some disadvantages, such as being costly requiring a lot of electricity, producing a lot of hazardous waste, etc (Oladoye et al., 2022).

Among the AOP, photocatalysis is capable of efficiently breaking down dyes and extracting them from wastewater without creating sludge. Subsequent to light irradiation, a semiconductor-based photocatalyst produces pairs of electrons and holes when electrons move from the valence band into the conduction band. Electron-hole pairs produced by photons will go to the surface of the semiconductor and experience a redox reaction (Mohamed et al., 2012). Superoxide radical anions ($^{\bullet}O_2^-$) are produced when the electron in the conduction band reacts with oxygen, while hydroxyl radicals ($OH^{\bullet}$) are easily produced by the hole created in the valance band with H_2O. According to (Majumdar & Pal, 2020), ROS are hydroxyl radicals ($OH^{\bullet}$) and superoxide radical anions ($^{\bullet}O_2^-$) that break down dyes and turn them into mineralized forms such as CO_2, H_2O, and other degradation products.

Titanium dioxide (TiO_2) has been utilised as a photocatalyst in most photocatalytic dye degradation experiments; nevertheless, TiO_2's primary drawback is that, because of its

large band gap, it only absorbs the UV component of light (Viswanathan, 2017). Similar to ZnO, which is also a commonly utilised photocatalyst due to its wide availability and non-toxic nature, its operational range is limited to the UV due to its wide band gap (Zhao et al., 2014). Particularly TiO_2 and ZnO are employed as thin porous films, nanorods, nanospheres, nanofibers, and nanowires, or as supports for polymeric films. Nanoscale zinc oxide is an inexpensive semiconductor with minimal environmental impact and low toxicity. Compared to TiO_2, it generates hydroxyl ions more effectively, producing emissions that are visible (Jana & Gregory, 2020). However, there are several disadvantages to ZnO, such as a high rate of electron-hole recombination (Anwer et al., 2019). They are unsuitable for large-scale applications because of their enormous band gap, quick charge recombination rates, and limited sensitivity to UV light (high *hv*), which makes up only 4-5 percent of the solar spectrum. The most favourable and long-term solution for dye degradation seems to be a narrow band gap photocatalyst sensitive to visible light (low *hv*), which makes up about 52% of the solar spectrum.

However, in recent years, a number of bismuth-based compounds have been developed as photocatalytic materials to use the visible spectrum. These include the Aurivillius structure (Bi_2MoO_6 (Cai et al., 2018), $Bi_4V_2O_{11}$ (Liang et al., 2018), $Bi_7Fe_3Ti_3O_{21}$ (X. Li et al., 2014)), Sillén structure (BiOCl (Y. Xu et al., 2018), BiOBr, BiOI [(Wu et al., 2015), (Arumugam & Choi, 2020)]), and Bi-based oxychloride ($Bi(IO_3)_3$ (H. Huang et al., 2018), $Bi_{12}O_{17}Br_2$, $Bi_4O_5Br_2$ (W. Zhang et al., 2017), Bi_3O_4Cl (Lin et al., 2007a), $PbBiO_2Cl$ (Yu et al., 2015)). The layers that make up the Aurivillius structure are $(Bi_2O_2)^{2+}$ lawers and perovskitic layers $(A_{n-1}B_nO_{3n+1})^{2-}$, with the $(Bi_2O_2)^{2+}$ layers situated in between the perovskitic layers. The production and separation of charge carriers under light were found to be facilitated by this hierarchical molecular structure, which is important for enhancing photocatalytic activity. As a new type of photocatalysts, Bi_4NbO_8Cl are layered semiconductors that are part of the Sillén and Aurivillius phases. They are composed of a layer of $(Bi_2O_2)^{2+}$ slabs interspersed with anionic $(NbO_4)^{3-}$ and Cl^- slabs (Ni et al., 2019). There is a significant internal electrostatic field between the slab layers that is perpendicular to the slab layers because of their distinctive layered structure. Consequently, the internal static electrical fields (IEF) can significantly enhance the separation of photoinduced electrons and holes, leading to the achievement of high photocatalytic activity for Bi_4NbO_8Cl (Ni et al., 2019). The first study to reveal that Bi_4NbO_8Cl is more active at breaking down methyl orange under visible light than anatase TiO_2 was done in 2007 by Lin and colleagues (Lin et al., 2007b). Hironori Fujito used theoretical and experimental

methods to demonstrate that Bi_4NbO_8Cl is a stable photocatalyst for the oxidation of water in visible light (Fujito et al., 2016).

Graphitic carbon nitride, or g-C_3N_4, has drawn a lot of interest recently in photocatalysis because of its tiny band gap (2.7 eV), which enables it to absorb visible light with no modifications (He et al., 2015). The popularity of this metal-free polymeric semiconductor can be attributed to a number of factors, including its low cost, ease of fabrication, remarkable chemical stability, increased electrochemical performance, and ecologically benign nature (X. Zhang et al., 2013) It is used for chemical synthesis, water splitting, CO_2 reduction, and organic pollutant degradation under visible light (Ou et al., 2017). However, the rapid recombination of photo-generated charge-carriers causes g-C_3N_4's low quantum yield, which restricts its practical use. To address this, numerous researchers have created g-C_3N_4 nanocomposites by combining it with other materials, such as WO_3/g-C_3N_4 (S. Chen et al., 2014), Bi_2O_3/g-C_3N_4 (J. Zhang et al., 2014), $BiVO_4$/g-C_3N_4 (Guo et al., 2014), Fe_3O_4/g-C_3N_4 (Kumar et al., 2013), In_2S_3/g-C_3N_4 (Xing et al., 2014), Bi_3O_4Cl/g-C_3N_4 (Ma et al., 2017), and g-C_3N_4/Bi_4NbO_8Cl (Majumdar & Pal, 2020) etc. These nanocomposites are superior to single semiconductors in terms of electron and hole separation and recombination reduction.

This study involved three main steps: the synthesis of Bi_4NbO_8Cl was carried out under control using a facile molten salt aided assembly approach; the synthesis of g-C_3N_4 was carried out using a calcine method; and finally, a hydrothermal method was used to build a nanocomposites of Bi_4NbO_8Cl/g-C_3N_4. The photocatalytic performance of the as synthesised photocatalyst is determined towards the degradation of Methylene Blue (MB) dye under a low-intensity, energy-efficient visible 20W LED light irradiation. The Bi_4NbO_8Cl/g-C_3N_4 nanocomposite was shown to have a considerably greater photocatalytic efficiency than both pure Bi_4NbO_8Cl and g-C_3N_4. The precise mechanism of the Bi_4NbO_8Cl/g-C_3N_4 nanocomposite's photocatalytic degradation of MB was further examined in order to obtain understanding.

1.2 OBJECTIVE AND SCOPE OF WORK

The study's goal is to economically and effectively remove MB from an aquatic matrix using a novel, non-toxic Bi_4NbO_8Cl/g-C_3N_4 nanocomposite photocatalyst when exposed to visible LED light. In order to accomplish this goal, the study's scope is as follows:

- The synthesis of a new Bi_4NbO_8Cl/g-C_3N_4 nanocomposite that has a different mass ratio between Bi_4NbO_8Cl and g-C_3N_4.
- Finding the most effective nanocomposites by conducting batch-mode research using the as-synthesised nanocomposites for the photocatalytic degradation of MB dye.
- Analysing the produced photocatalyst using different methods to understand its material characteristics.
- Optimization of process parameters for the photocatalytic degradation and mineralization of MB.
- Find out the photocatalyst's photocatalysis mechanism and reaction kinetics in order to remove MB.

Chapter 2

2. LITERATURE REVIEW

2.1. DYES AND IT'S CLASSIFICATION:

A dye is a coloured substance that has an affinity for the substrate to which it is being applied. It absorbs light at a specific wavelength in the visible portion of the spectrum, which is why it is coloured. Dye is an ionizing and aromatic organic compound. Usually applied in an aqueous solution, the dye may need to be treated with a mordant to increase its fastness on the fibre. There is rarely a sector that does not employ colours commercially—from plastic toys to clothing, from food to wood. Dye is applied everywhere. In essence, dyes are aromatic, ionising substances with various chromophore molecules that give them their colour. The aryl rings in their structures feature electron systems that are delocalized. (Natarajan et al., 2018a). Dyes can be classified in several ways; each class has a very unique chemistry, structure and particular way of bonding. While certain dyes can be held in place by physical forces, others can react chemically with the substrates to produce strong connections. The dye classification is displayed in Fig. 1. Dyes can be categorised according to how they are made, what materials are used in their synthesis, the characteristics of each dye's chromophores, and the type of electronic excitation. Dyes can be natural as well as synthetic. Natural sources such as plants (including lichens and fungi), animals, invertebrates, and minerals are the source of natural dyes. Some of the examples of natural dyes are Indigo dyes (from stems and leaves of indigo), Alizarin dyes (from roots of madder plant), Logwoods dyes (from the trunk for black colour to silk and cotton fabrics) etc. In nature, these dyes don't pose much of a threat. For the purpose of dyeing, synthetic dyes are made in laboratories or factories. A few examples of synthetic dyes are azo and mordant dyes. Today, synthetic dyes predominate because they are more readily obtainable, less expensive, faster to set, brighter, and come in a broader variety of hues. In nature, these artificial dyes are poisonous. It can pose a number of health risks to people if it is found in water sources. A variety of organic dyes with different chemical structures, including thiazine, xanthene, anthraquinone, phenanthrene, quinoline, indigo, triphenylmethane, and azo dyes, have been examined by Epling and Lin (2002) in relation to visible light assisted degradation (Epling & Lin, 2002).

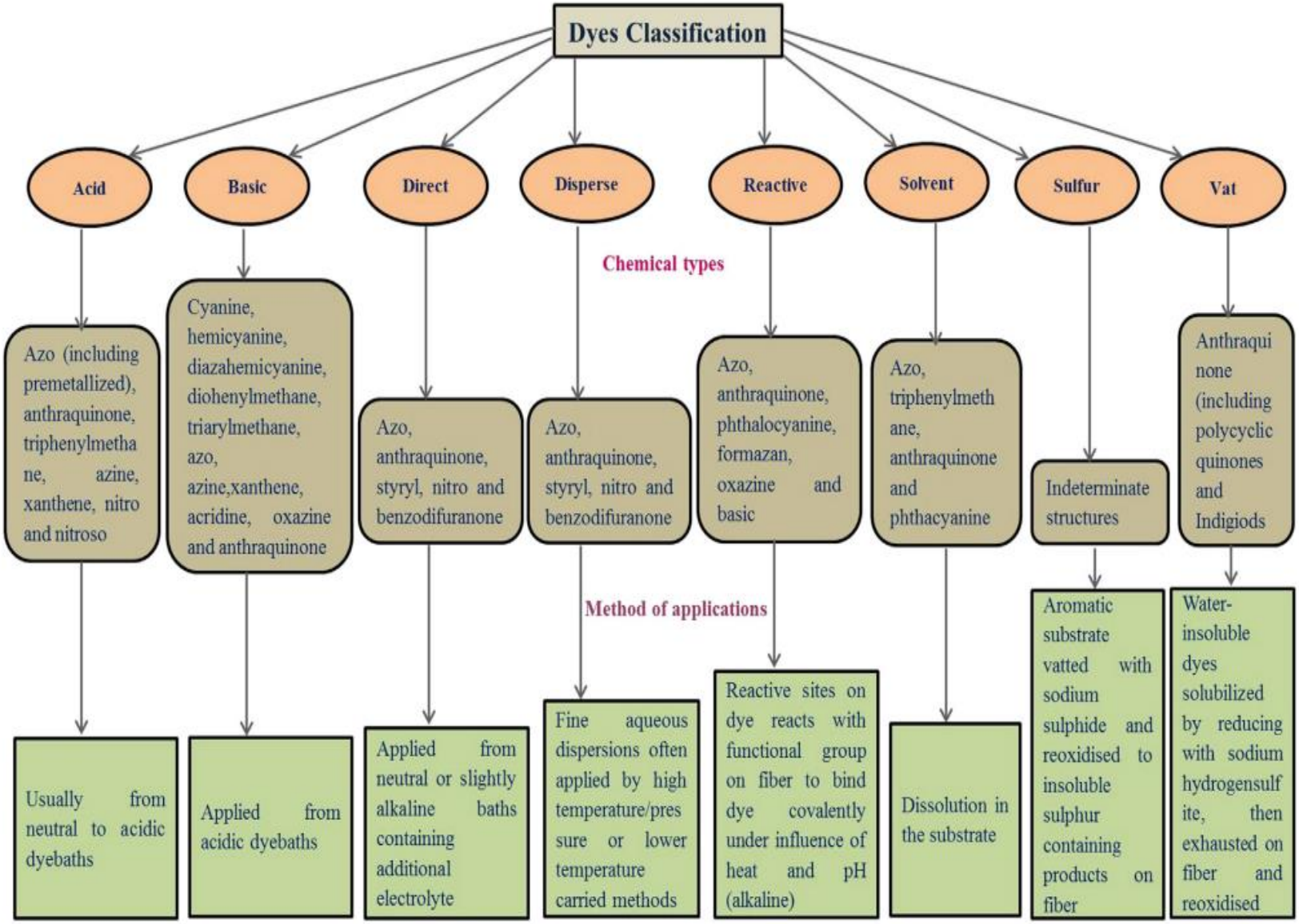

Fig. 1 – Classification, applications and method of applications of dyes.

2.1.1. Cationic dyes:

In an aqueous solution, a cationic functional group found in cationic dyes may dissolve into positively charged ions. The most prevalent cationic functional group is the onium group. Catalytic dyes, wherein the majority of the cations are N^+, include Methylene Blue (MB), Rhodamine B (Rh B), Rhodamine 6G (Rh 6G), Safranin O (SO), Crystal Violet (CV), and Malachite Green (MG). Consequently, basic dyes are another name for cationic dyes. As a model contaminant for degradation, MB was employed. MB is safe and helpful when administered as medicine at a safe concentration. However, the aquatic biota and human health may be negatively impacted in multiple ways by the careless release of MB into a waterbody. The health risk related to coming into contact with MB include impacts on the central nervous system, gastrointestinal tract, respiratory system, cardiovascular system, genitourinary problems, and skin (Oladoye et al., 2022). Fig: 2

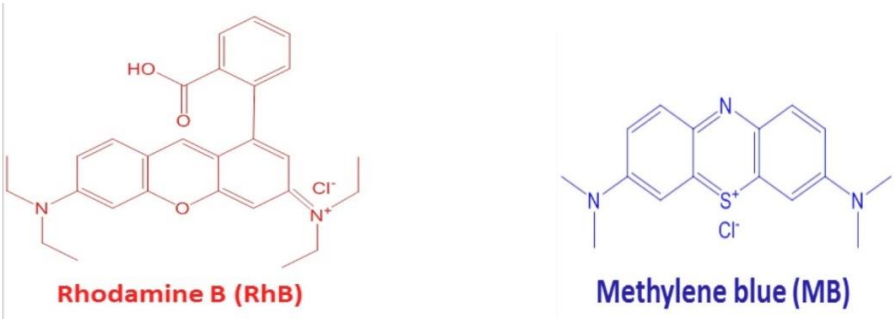

Fig. 2. Cationic dye

2.1.2. Anionic dyes:

Anionic dyes contain anionic functional groups (e.g., sulfonic or carboxylic acid groups) that are water soluble and may interact easily with photocatalysts with hydrophilic surfaces. As a result, anionic dyes are sometimes called acidic dyes. Some of the anionic dyes are Acid Orange 7 (AO7), Eosin Y (EY), Methyl Orange (MO), Fluorescein sodium salt, Potassium Permanganate, Acid Red 14 (AR14), Alizarin Red S (ARS), Rose Bengal (RB), and Phenol Red (PR) (Sanakousar et al., 2022). Fig: 3

Fig. 3: Anionic dye

2.1.3 Non-ionic Dyes:

I. Disperse dyes:

Disperse dye is described as a substantially water insoluble dye associated with one or more than one hydrophobic nature of fibers, such as polyester or cellulose acetate. As disperse dye is non-ionic, it is easily volatile and vapors of dye are highly absorbed by the hydrophobic fiber. Some examples of dispersed dyes are C.I. Disperse Yellow 13 which is suitable for acetates and nylon, C.I. Disperse Violet 1 which is suitable for acetate, nylon and polyester, C.I. Disperse Blue 56 which is suitable for dyeing polyester fibers, C.I. Disperse Orange 30 which is applied on acetate and triacetate, C.I. Disperse Blue 183 for dying of polyester. The chemical structure of some dispersed dyes are shown in Fig. 4 (Clark, 2011).

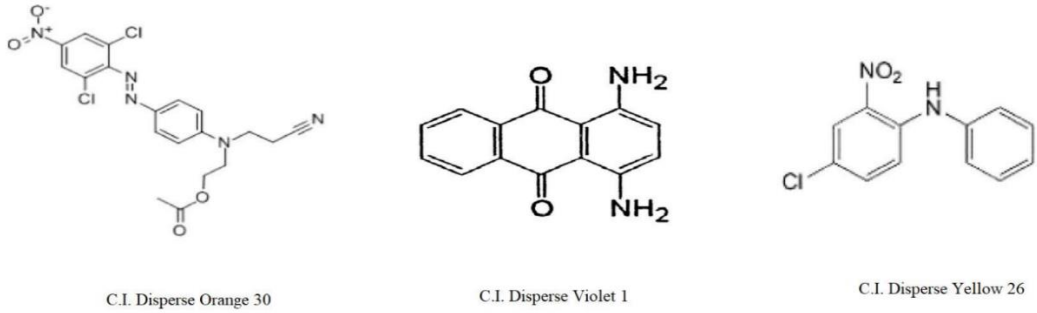

Fig. 4: Disperse dye

II. Vat dye:

Vat dye is identified for better color fastness and excellent brightness properties. They are primarily soluble in hot water and some vat dyes are also soluble in sodium carbonate. The most important natural vat dye is Indigo or indigotin obtained from the plant Indigofera. some of the vat dyes are C.I. Vat Blue 1, C.I. Vat Black 25, C.I. Vat Green 1. The chemical structure of some vat dyes is shown in Fig. 5 (Sharma et al., 2021).

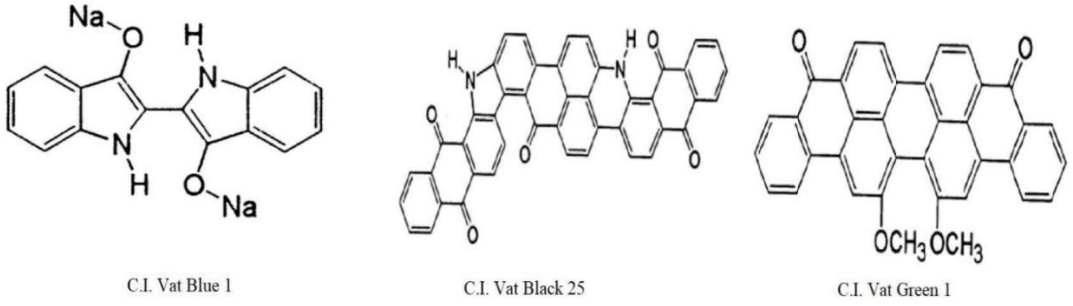

Fig.5: Vat dye

III. Sulfur dyes:

Sulfur dyes are highly coloured, water insoluble compounds. They are the most commonly used dyes manufactured for cotton in terms of volume. Sulfur dyes are predominantly black, brown, and dark blue. These dyes are categorized into four groups such as sulfur, Leuco sulfur, solubilized and condensed sulfur dyes. Some of the sulfur dyes are Sulfur Blue dye, CI 53235, Sulfur Black, CI 53185, Leuco Sulfur Black1, CI 53185, Sulfur brilliant green, CI 53570. The chemical structure of some sulfur dyes are shown in Fig. 6 (Sharma et al., 2021).

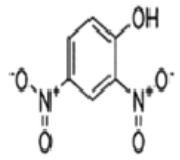

Sulfur black, CI 53185

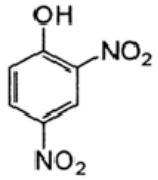

Leuco Sulfur black 1, CI 53185

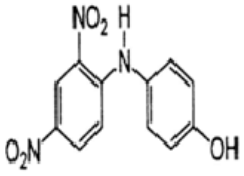

Sulfur blue dye, CI 53235

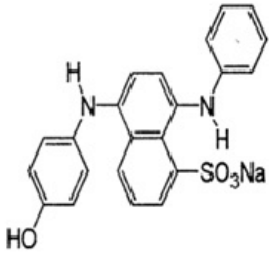

Sulfur brilliant green, CI 53570

Fig.6: Sulfur dye

2.2 ENVIRONMENTAL IMPACT OF DYES:

According to (Surolia et al., 2010), dye plays a significant role in our daily lives because it is utilised in a variety of industries, including the textile, leather tanning, paper, food, pharmaceutical, and medical fields, as well as in agricultural, biological, and chemical research, light-harvesting arrays, photo electrochemical cells, cosmetics, hair colouring, and wood stanning. According to Zollinger, roughly 450,000 tonnes of dyestuff are produced worldwide, and about 40,000 different synthetic dyes and pigments are employed in various industries. The textile sector is the biggest user of these dyes, making up around 65% of the market (Zollinger H., 1987). According to a survey conducted by the

Ecological and Toxicological Association of Dyestuffs and Manufacturing Industry (ETAD), 90% of the 4000 dyes that were screened were found to have lethal doses (LD50) greater than 2 × 103 mg/kg. Direct, basic, and di-azo dyes had the highest rates of toxicity among the dyes that were tested. It is evident from the literature that water soluble dyes with vibrant colours, such reactive and acid dyes, are challenging to eliminate from water (Beyene, 2014). Drinking water tainted with these substances can have a range of detrimental effects on human health, including extensive immune suppression, respiratory issues, disorders of the central nervous system (CNS), allergic reactions, tissue necrosis, and infections of the skin and eyes (Pan et al., 2012) (Fig 7). Highly carcinogenic or mutagenic chemicals can arise during the reduction of dyes and their intermediates, which is harmful to aquatic life and microbes (Carliell et al., 1996). Therefore, it is crucial to remove the dye from wastewater by reducing or eliminating its toxicity in addition to removing the dye's colour from the water (Natarajan et al., 2018b).

Government regulations pertaining to the removal of dyes from industrial effluents have been stricter recently in both developed and developing nations, and law enforcement will persist to guarantee that the effluent from dye-utilizing industries meets the necessary standards (Anjaneyulu et al., 2005)

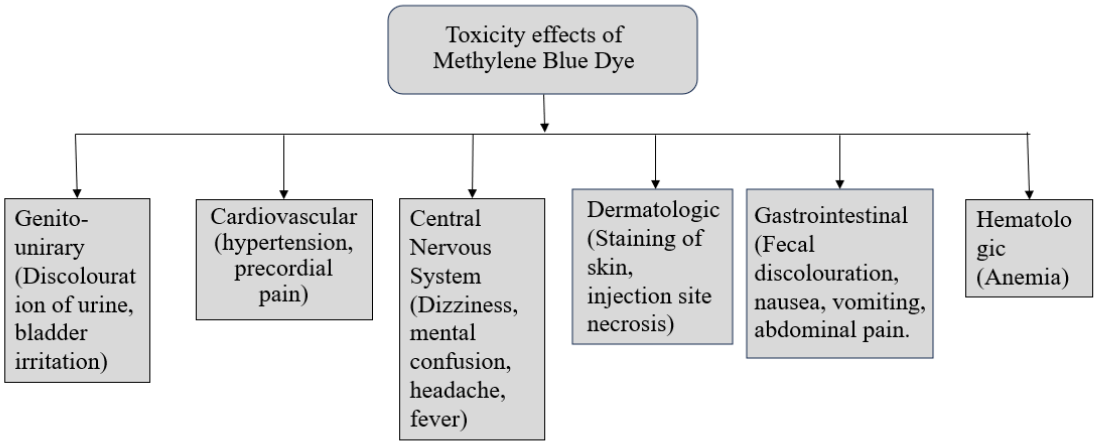

Fig.7: Toxicity Effect of Methylene Blue Dye

2.3. AVAILABLE TECHNOLOGIES FOR REMOVAL OF DYES:

Most synthetic dyes are toxic by nature and pose a threat to aquatic life. Numerous conventional techniques have been employed to remove colour from water and wastewater in order to comply with strict environmental regulations. These techniques are arranged according to Figure 8.

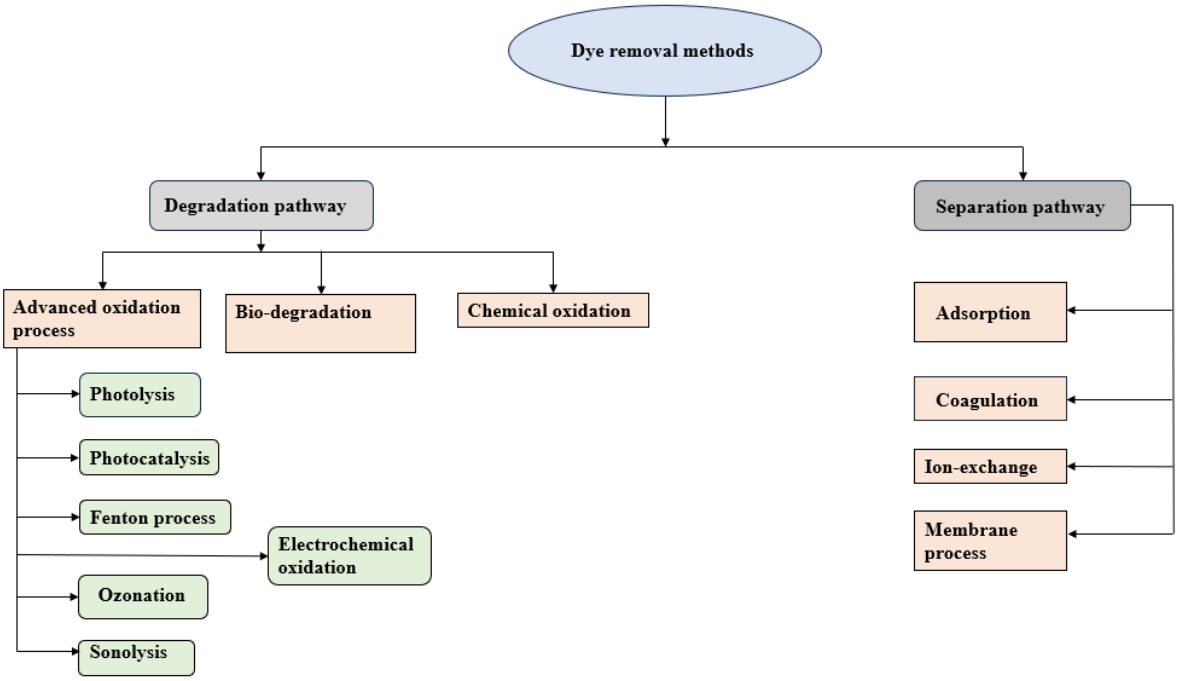

Fig.8: Various methods for dye removal

2.3.1 Chemical coagulation & flocculation:

The physicochemical processes of coagulation and flocculation are frequently used to clean industrial wastewater because they destabilise and produce flocs, which eliminate colloidal particles, minuscule solid suspensions, and a few soluble chemicals that were previously present in the wastewater. The coagulation process is one of the easiest and least expensive methods that can be used in industrial settings, and it has also been shown to be the most successful strategy when compared to other processes like anaerobic reduction, oxidation, and adsorption (Kos, 2016). About 70–80% of the colour is removed during coagulation, and the amount of organic chemical concentration is decreased by the same amount. The characteristics of the raw wastewater, the temperature and pH of the solution, the kind and amount of coagulants employed, and the amount of time spent mixing all affect how effective this process is (Mokif, 2019). Common coagulants include synthetic organic polymers and inorganic

salts like ferric chloride or alum. Chemical coagulants have several disadvantages, including the potential to induce disorders like Alzheimer's disease, which is linked to inorganic salts, and the fact that some of them are carcinogenic. Despite being used to remove suspended particles and colours from wastewater, they have several negative effects.

Understanding a coagulant's performance under particular conditions is essential since chemical coagulation is a complicated process with many interrelated properties. Alum, ferric chloride, ferric sulphate, and magnesium chloride can all be used as a coagulant. Distinct coagulants have various effects on destabilisation. The more destabilising and the lower the needed coagulation dose, the higher the counter ion's valence. When the pH is lower than the isoelectric point of metal hydroxide and various coagulants are precipitated by a suitable polymer, positively charged polymers will be more prevalent. Through charge neutralisation, the adsorption of these positively charged polymers can cause negatively charged colloids to become unstable. Above the isoelectric point, where particle instability may arise from adsorption and bridge formation, anionic polymers will predominate. The use of a substantial dose of metal ions (coagulant) causes an adequate level of oversaturation, which causes a large amount of metal hydroxide to precipitate quickly and enmeshing the colloidal particles known as sweep flocs. When Fe (III) salts are utilised as coagulants, monomeric and polymeric ferric species are generated; the production of these species is pH dependant. Numerous investigations have shown that ferric chloride solutions have an acidic natural colour. However, effective removal of the acidic substance is only possible when the pH is near neutral, necessitating the addition of a base to maintain pH stability. This can be accomplished with lime or sodium hydroxide (NaOH). Conversely, lime can produce more sludge. On the other hand, using polyelectrolyte as a coagulant aid frequently enhances the coagulant's functionality. As can be seen, alum works best at a pH that is almost neutral, which maximises the effectiveness of colour removal. Additionally, adding polyelectrolyte enhances colour removal effectiveness overall. This method is not pleasant, though, because it produces a lot of sludge. The ideal pH range for magnesium chloride is 9 to 12. When used with lime, it offers superior colour removal. But it generates a lot of sludge, which could lead to extra expenses and a problem with sludge disposal. While alum and ferric chloride both have excellent effectiveness, ferric chloride is less successful at removing colour at low doses. However, there has been a noticeable improvement in colour removal when ferric chloride is mixed with a little amount of cationic polymer.

2.3.2 Electro coagulation:

Colour removal from wastewater using electrochemical technology is one application of the electro coagulation process. This technology attracted a lot of attention because to its special qualities of safety, adaptability, and compatibility with the environment. Electrochemical technology competes with other conventional technologies including ion exchange, solvent extraction, evaporation, and precipitation to suit the demands of many sectors. Because electrochemical methods use the electron as a single reagent and do not leave behind solid residues, they are often preferable to physicochemical and membrane technologies, particularly when it comes to eliminating colour from wastewater. During electro coagulation, the primary techniques for removing pollutants are flotation, adsorption, coagulation, and precipitation. Compared to chemical coagulation, electro coagulation produces less sludge, has a smaller environmental imprint because of its quicker reaction time, requires less equipment and operating costs, and is simpler to use.

During electrocoagulation, the electrooxidation of sacrificial anodes produces coagulants in situ. After that, the precipitates or suspended particles are destabilised and aggregated by iron or aluminium hydroxide flocs, which absorb dissolved pollutants. Iron and aluminium are the most often utilised materials in electrocoagulation because they are easily accessible and reasonably priced. Dalvand et al. looked into the efficacy of electrocoagulation using aluminium electrodes to extract Reactive Red198 (RR198) from aqueous solution. The effect of variables on the percentage of dye removal was examined (Dalvand et al., 2011a). These variables included voltage variation, reaction duration, inter electrode distance, initial dye concentration, electrolyte concentration, and electrode connection mode. In terms of electrode and electrical energy consumption, they also investigated the optimal operating parameters. Several groups make up Reactive Red198's (RR198) organisational structure. These groups contain three distinct absorbance peaks at 288, 373, and 518 nm. It is possible to assign the benzene, naphthalene, and azo-linkage peaks to, respectively, benzene, naphthalene rings, and azo-linkage. The breakdown of dye molecules into smaller organic compounds may be the cause of dye loss during electrochemical processes, depending on the type of electrode material utilised. The absorbance of raw and treated wastewater was measured at three absorption wavelengths: 288, 373, and 518 nm, in order to evaluate the dye removal method by electrocoagulation. Furthermore, to ascertain whether aromatic compounds resulting from dye breakage were present in the solution, absorbance at 254 nm was assessed. All of the absorbance peaks dropped throughout the electrocoagulation treatment and vanished nearly entirely after thirty minutes or so. The principal mechanism for dye

removal was found to be dye molecule adsorption on flocs, as demonstrated by the decrease in absorbance peaks. No other byproducts were produced or azo-linkage cleavage occurred as a result of the removal of RR198. The cleavage azo group's minimal involvement in dye removal is confirmed by the high rate of COD elimination (84.1%). The decreased COD removal relative to dye removal may be explained by the poor electro-oxidation-mediated breakdown of dye molecules into tiny organic compounds.

2.3.3 Membrane process (Reverse Osmosis (RO) & Nano Filtration (NF)):

Membranes are frequently utilised in a number of separation processes due to their capacity to control the materials going through them, resulting in a high degree of separation that is always attained, making these processes broadly accepted. The membrane functions as a barrier, allowing certain chemicals to permeate through it while restricting others from doing so in a certain way (retentate). Fluids, dissolved solids, suspended solids, and colloidal dissolved solids can all be separated using membranes. The primary features of membrane processes in the consumables treatment industry are their capacity to extract or recover valuable or toxic components and to shut off water systems, hence lowering fresh water use.

Wastewater can be cleansed to a degree that is impossible to reach with conventional procedures thanks to the employment of membrane technologies. The two most popular and important membrane filtering methods are reverse osmosis (RO) and nanofiltration (NF). The membrane pore size of NF is between 0.5 and 2 nm, and its operating pressure ranges from 5 to 40 bars. It is used to separate monovalent salts, ions, and water from sugars, other organic molecules, and multivalent salts. On the other hand, it is used to separate monovalent salts from water. The membrane pore size in RO or hyper filtration is about 0.5 nm. In a RO, operating pressures typically range from 7 to 100 bars. The membrane areas that are deployed in different industrial sectors serve as evidence of the significance of membrane processes. Because RO membranes can remove both organic and inorganic chemicals, they are a popular option for treating contaminated drinking water supplies. Reverse osmosis can be used to concurrently remove a range of contaminants, including organic pollutants like agricultural pesticides and tri-halo methane precursors, as well as hardness, colour, germs, viruses, and more. In order to minimise the quantity of water discarded and enable the treated water to be reused, Avlonitis et al. examined effluents from the cotton textile sector that were treated using a nanofiltration membrane (S. A. Avlonitis et al., 2008). The outcomes shown that NF membranes could entirely remove colour from the cotton dye

effluent and lower the overall salt content by over 72%. These membranes have the ability to provide reusable, high-quality water even at low pressures and high recoveries. Gozálvez-Zafrilla et al. investigated wastewater reuse in the textile sector by treating secondary wastewater (Gozálvez-Zafrilla et al., 2008). They conducted their investigation using (NF90) membrane. The findings revealed that NF90 had 99 percent COD reduction (75–95%) and the highest salt rejection. Fouling had little effect on the levels of COD removal or salt rejection, and the permeate quality permitted a high flux percentage to be recovered following cleaning. Acid red, reactive black, and reactive blue dye were tested by Abid et al. using the RO & NF method (Abid et al., 2012). They found that dye could be successfully removed from wastewater using RO and NF membranes, and that the amount of dye removed depended on the pH, TDS, applied pressure, and amount of dye in the feed solution, but not on feed temperature.

2.3.4 Biological process:

Microorganisms including fungi, bacteria, and algae are used in the biological process because they can biodegrade and absorb pigments present in wastewater. The application of microorganisms for wastewater colour removal has several benefits, such as low cost, ecologically friendly method that generates less secondary sludge, and nontoxic end products for full mineralization. Numerous studies have demonstrated the capacity of bacteria such as Citrobacter sp., Aspergillus niger, Bacillus cereus, Chlorella Spand, and Cunninghamellaelegans to extract dye from industrial wastewater. The adaptability and activity of each microbe are the main elements influencing the decolorization efficacy of microbial activity. Although biological treatment is used to remove colour, conventional aerobic therapy is less likely to be used for dye removal because most dyes are made to withstand light and oxidation deterioration. One specific issue is the elimination of colours that are soluble in water by aerobic processes. Some of these pigments are adsorbed on sludge from wastewater. Although direct biological treatment with bacteria or fungus is also an option, the use of these bioremediation techniques is limited by the nutritional and physiological needs of microorganisms. Research into efficient and eco-friendly oxidation procedures has led to an increase in the usage of enzymes to substitute conventional non-biological methods. It has been demonstrated that treating textile azo dyes biologically is an efficient way to break down all dye components and get beyond many of the drawbacks associated with physicochemical methods. Microbes and their enzymes can break down dye through both aerobic and anaerobic metabolism. Numerous research on the breakdown of environmental pollutants by various bacteria

have been published. Numerous bacteria have been shown to be hydrocarbon-only feeders. Hydrocarbons can be broken down by bacteria that have hydrocarbon-degrading bacteria. These biodegradable and easily maintained bacterial bio flocculants offer a cost-effective and environmentally friendly substitute for or addition to existing treatment methods for the removal of colours from wastewater effluents. The capacity of microalgae Cosmarium species to decolorize a solution containing the cationic textile dye Malachite Green was investigated by Daneshvar et al. (Daneshvar et al., 2007). Along with examining the relationship between kinetic characteristics and dye concentration and other rate-dependent environmental factors (temperature, pH, algal concentration, and dye concentration), they also examined algal resilience and reusability throughout multiple decolorization operations.

2.3.5 Adsorption with conventional adsorbent (activated carbon):

Among the numerous dye removal procedures available, adsorption is the method of choice that yields the greatest results since it can be used to remove a wide range of colouring materials. A well-designed adsorption system will result in high-quality treated effluent. Adsorption processes can be categorised as physical or chemical depending on the type of forces at play. The adsorption process is influenced by a number of physico-chemical parameters, including particle size, pH, temperature, contact time, adsorbent surface area and pore structure, surface chemistry, type of the adsorbate, and the effect of other ions. The adsorption approach has shown to be more practical and effective than other methods including coagulation, flocculation, precipitation, and activated sludge because of its low cost, straightforward design, ease of handling, and sludge-free cleaning processes. Treatment options such as adsorption techniques are feasible, especially if the adsorbent is inexpensive and easily accessible. Among commercial adsorbents, activated carbon is the most commonly utilised adsorbent. It has been noted that using activated carbon as a dye removal method is a practical choice. Because of its distinct molecular structure, activated carbon has an incredibly high affinity for a wide range of dyes, including basic dyes. Activated carbon is utilised as a sorbent in the majority of commercial systems to remove colours from wastewater because of its great adsorption capabilities. The US Environmental Protection Agency lists activated carbon adsorption as one of the finest control strategies currently in use (Dias et al., 2007). On the other hand, activated carbon is a better sorbent, but its expensive cost prevents it from being used widely. An attempt has been made to lower treatment costs by locating inexpensive substitute adsorbents. El Qada et al. looked into activated carbon and evaluated the adsorption capacities of

three distinct activated carbons: commercially available Filtrasorb 400, and PAC1 and PAC2, which were developed at QUB for this study (El Qada et al., 2008). Because basic dyes are toxic, have a very high tinctorial value (less than 1 ppm of dye visible in solution), and ionise in solution to form cations that have a strong affinity for negatively charged adsorbent surfaces, they were selected as the model adsorbates.

2.3.6 Adsorption with conventional adsorbent (fly ash):

Many strategies for creating less expensive and more potent adsorbents have been researched in addition to conventional adsorbents like activated carbon. Numerous non-conventional low-cost adsorbents, such as natural materials, biosorbents, and waste products from industry and agriculture, have been proposed by several researchers. As sorbents, these substances could be employed to extract colours from solutions. It has been reported that sorbents include: biosorbents (chitosan, peat, biomass); clay materials (bentonite, kaolinite); zeolites; siliceous materials (silica beads, alunite, perlite); agricultural wastes (bagasse pith, maize cob, rice husk, coconut shell); industrial waste products (waste carbon slurries, metal hydroxide sludge); and others (starch, cotton, and so on). The technological viability of employing unconventional, inexpensive adsorbents to extract colour from tainted wastewater was examined by G. Crini (Crini, 2006). He thinks there's a great deal of commercial potential for low-cost adsorbents in the future. When compared to activated carbon, chitosan-basedsorbents in particular have shown to have better dye removal properties. There is still a dearth of data with a thorough comparison of sorbents, even in spite of the publication of several studies on inexpensive adsorbents. Even though the field of low-cost sorbents has advanced significantly, much more work is still required to: (i) better understand adsorption mechanisms; (ii) predict the performance of adsorption processes for dye removal from actual industrial effluents under a range of operating conditions; and (iii) demonstrate the use of low-cost sorbents on an industrial scale. Mohan et al. utilised fly ash produced in thermal power plants as a low-cost adsorbent for the removal of crystal violet and rosaniline hydrochloride (basic fuchsine) from wastewater (Mohan et al., 2002). They found that the two dyes' adsorption increased with temperature, suggesting that the process is endothermic. The results show that the Freundlich and Langmuir models may both be used to fit the data and estimate model parameters. In general, the data is better fitted by the nonlinear Freundlich adsorption isotherm. When applied to fly ash, the adsorption capabilities of crystal violet and basic fuchsine dyes are either higher or comparable to those of other adsorbents used with the same or different cationic dyes. Their results indicate that fly ash is a useful

adsorbent for the removal of dyes.

2.3.7 Advanced oxidation process (AOP):

In low concentrations or when they are very resistant to oxidants, dyestuffs and organic compounds with complex structures have proven difficult to oxidise using conventional oxidation methods. To address the aforementioned issues, advanced oxidation processes, or AOPs, have been created to produce hydroxyl free radicals through a variety of methods. The most promising methods for treating textile wastewater are AOPS procedures, which combine UV irradiation, hydrogen peroxide (H_2O_2), and ozone (O_3). While these oxidants were successful in decolorizing dyes, COD was not entirely removed. The aim of any AOP is to produce and employ hydroxyl free radical ($OH^{\bullet}$) as a potent oxidant to break down substances that are resistant to traditional oxidants. The generation of $OH^{\bullet}$ radicals and attack selectivity a valuable characteristic of an oxidant define advanced oxidation processes. AOP's adaptability is increased by the fact that it can be applied to $OH^{\bullet}$ in a number of ways. It is usual practice to combine O_3, H_2O_2, TiO_2, UV radiation, electron beam irradiation, and ultrasound to accelerate the generation of $OH^{\bullet}$. For oxidising textile wastewater, O_3/H_2O_2, O_3/UV, and H_2O_2/UV show the most promise. The table below compiles the many dye removal procedure types, important variables, removal efficiency, benefits, and drawbacks.

Table 1: Different types of dye removal processes

Technology	Target Dye	Significant factors	Results	Advantages / Disadvantages	References
Chemical Coagulation	Reactive dye, sulfur dye, acid dye, disperse dye,	(i) Optimum dose of coagulant: alum, magnesium chloride, ferric chloride, ferrous sulfate	Reactive dye: 98% (alum), 71% (ferric chloride), 90% (ferrous sulfate), 85% (magnesium	Advantages: It is an economically feasible process and efficiently removes the colour from wastewater	(Tan et al., 2000) (Georgiou et al., 2003) (Golob et al., 2005) (Bidhendi et al.,

		(ii) Coagulant aids: Poly-acrylamide based polymer is used with alum &Polyelectrolyte Can be used for ferric chloride, magnesium chloride & ferrous sulfate (iii) pH of the solution: alum (5.3-7), ferrous sulfate-(9.4-12.5), ferric chloride-(6 8.3), magnesium chloride-(11-12)	chloride) Disperse dye: 78.9% (alum), 71% (ferric chloride), 98% (magnesium chloride) Sulfur dye: 100% (ferric chloride), 90% (ferrous sulfate) Acid dye: 98% (alum)	Disadvantages: Huge sludge production is the major disadvantage of this process	2007) (Gao et al., 2017a)
Electro coagulation	reactive red 198	voltage, electrode connection mode, electrical energy consumption, inter electrode distance, dye concentration and	i) Dye removal follows first order kinetics; ii) 98.6% dye removal and 84% COD removal;	Advantages: requires smaller space, easy operation, eco-friendly process, cost effective method; Disadvantages: sludge Generation	(Kobya et al., 2007) (Dalvand et al., 2011b) (Latha et al., 2017)

		electrolyte concentration;			
Membrane processes: reverse osmosis (RO), nano filtration (NF)	acid red, reactive blue, reactive black,	RO: membrane pore size (0.5 nm), operating pressure (7–100 bars); NF: membrane pore size (0.5–2 nm), operating pressure (5–40 bars);	i) NF method consumes half of the electrical power compared to RO; ii) NaCl in dye solution increases dye removal efficiency; iii) pH, TDS, applied pressure and dye concentration show good effect on dye removal; iv) Feed temperature shows bad effect on dye removal;	Advantages: higher removal potential with lower effective cost; Disadvantages: production of concentrated sludge;	(G. Avlonitis et al., 2008) (Gozálvez-Zafrilla et al., 2008) (Abid et al., 2012))
Biological processes: Green algae (Cosmarium species)	Malachite green	Dye concentration, Algal concentration, solution pH, and temperature	i) Dye decolourization rate is described with Michaelis-Menten model; ii) Optimum	Advantages: Algae are available in worldwide in different kinds of habitats, good capability for	(Crini, 2006) (Daneshvar et al., 2007)

			pH is 9; temperature (5–45 C) has positive effect on decolourization rate; iii) Optimal kinetic parameters: v_{max} (maximum specific decolourization rate) is 7.63 mg dye g cell–1h–1 and Km (dissociation constant) is 164.57 ppm;	verity of dye decolourization, economically feasible, publicly acceptable process; Disadvantages: slow process, needs to be performed under optimal favorable conditions;	
Activated carbon (AC) adsorption	Methylene blue, basic yellow 21, basic red 22	AC surface area, surface chemistry, pore structure; adsorbent dose, and solution pH;	i) Three adsorption isotherm models (Langmuir, Freundlich and Redlich-Peterson) have been used, Redlich-Peterson model gave best fit; ii) Alkaline pH and low pore	Advantages: very effective adsorbent, high adsorption capacity; Disadvantages: non-destructive process, AC regeneration is very costly;	(Crini, 2006) (El Qada et al., 2008)

			size of AC favored dye adsorption;		
Adsorption with non-conventional adsorbents: Fly ash from thermal power plant	Basic violet, Basic fuchsine	Adsorbent particle size, adsorbent dose, solution pH, and temperature;	i) Langmuir and Freundlich adsorption isotherm have been used, nonlinear Freundlich model gave better fit; ii) Negative free energy value and positive enthalpy value suggest spontaneous and endothermic process; iii) Dye adsorption follow 1storder kinetics;	Advantages: cost effective adsorbent, high adsorption capacity; Disadvantages: non - destructive process, expensive regeneration process;	(Crini, 2006) (Mohan et al., 2002)
Advanced oxidation processes (AOPs)	Several textile dyes	Ozone (O_3), hydrogen peroxide (H_2O_2), wavelength of ultraviolet (UV) light,	i) In O_3/UV process hydroxyl radical (OH•) is produced after	Advantages: complete mineralization achieved in presence of OH•; no sludge	(Al-Kdasi et al., 2004)

		O_3/UV, H_2O_2/UV, O_3/H_2O_2/UV, solution pH, dye concentration, and temperature;	activation of O_3 by UV(ƛ = 254 nm); ii) H_2O_2/UV also produces OH• radical for dye degradation; iii)Among all AOPs O_3/H_2O_2/UV shows highest efficiency for dye degradation;	generation, appropriate process for recalcitrant dyes; Disadvantages: several by product formations, less economic feasibility;	

AOP's adaptability is increased by the fact that it can be applied to $OH^{\bullet}$ in a number of ways. It is usual practice to combine O_3, H_2O_2, TiO_2, UV radiation, electron beam irradiation, and ultrasound to accelerate the generation of $OH^{\bullet}$. For oxidising textile wastewater, O_3/H_2O_2, O_3/UV, and H_2O_2/UV show the most promise. The table below compiles the many dye removal procedure types, important variables, removal efficiency, benefits, and drawbacks.

2.4 PHOTOCATALYSIS:

When photocatalytic mineralization for different halogenated hydrocarbons was accomplished successfully in the 1980s, photocatalysis for water purification was initially recognised (PRUDEN, 1983). In the Advanced Oxidation Process (AOP) known as photocatalysis, when exposed to under the influence of light, a semiconductor-based photocatalyst creates pairs of electrons holes when electrons move from the valence band into the conduction band. Electron hole pairs produced by photolysis will migrate towards the semiconductor's surface, where they will experience a redox process (Mohamed et al., 2012). The conduction band electron combines with oxygen to make superoxide radical anions ($^{\bullet}O_2^-$), and the hole created

in the valance bond readily reacts with H_2O to produce hydroxyl radicals ($OH^{\bullet}$). The following equations illustrate the process by which hydroxyl radicals and superoxide radical anions are produced.

$$\text{Photocatalyst} + h\upsilon \rightarrow e^-_{cb} + h^+_{vb} \quad \ldots.(1)$$

$$H_2O + h^+_{vb} \rightarrow OH^{\bullet} + H^+ \quad \ldots.(2)$$

$$OH^- + h^+_{vb} \rightarrow OH^{\bullet} \quad \ldots.(3)$$

$$OH^{\bullet} + OH^{\bullet} \rightarrow H_2O_2 \quad \ldots.(4)$$

$$H_2O_2 + h\upsilon \rightarrow 2OH^{\bullet} \quad \ldots.(5)$$

$$O_2 + e^-_{cb} \rightarrow {}^{\bullet}O_2^- \quad \ldots.(6)$$

$${}^{\bullet}O_2^- + H_2O_2 \rightarrow OH^{\bullet} + O_2 + OH^- \quad \ldots.(7)$$

$$H_2O_2 + e^-_{cb} \rightarrow OH^{\bullet} + OH^- \quad \ldots.(8)$$

Reactive oxygen species (ROS) are superoxide radical anions (${}^{\bullet}O_2^-$) and hydroxyl radicals ($OH^{\bullet}$) that break down dyes and produce CO_2, H_2O, and other degradation products. The illustrations of dye deterioration are displayed below in Fig. 9.

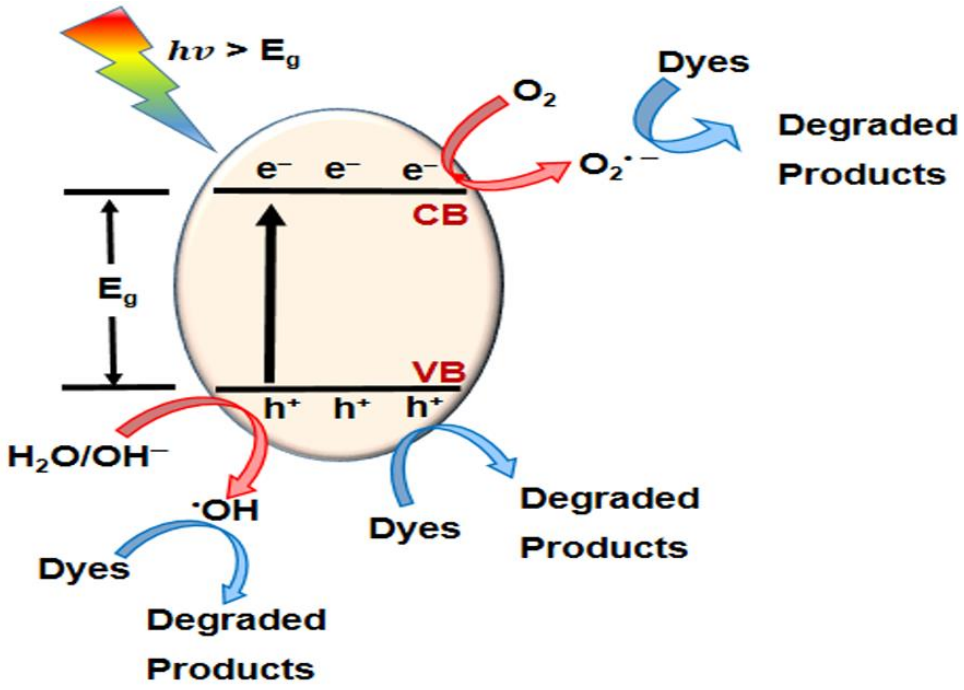

Fig: 9. Pictorial representation of the process taking place in the photocatalytic degradation of dyes on semiconductor surfaces

Three significant factors impact how well the photocatalyst degrades dye: (1) band-gap energy (Eg): Photocatalysts that have a broad band-gap are UV-sensitive, whereas those that have a narrow band-gap are visible-sensitive; (2) Band edge potentials, or VB and CB potentials: Only when the VB potential is more positive than the normal oxidation potential of $OH^{\bullet}/H_2O$ (+ 2.68 eV vs. NHE) or $OH^{\bullet}/OH^{-}$ (+ 1.99 eV vs. NHE) and/or the CB potential is smaller than the reduction potential of O_2 to $^{\bullet}O_2^{-}$ (− 0.33 eV vs. NHE) can ROS be produced(Panneri et al., 2017). In the event that this is not the case, the pollutant and the h^+ in the VB interact immediately. Recombination leads to the production of $^{\bullet}O_2^{-}$when the e returns to the VB without going through the reduction reaction (Pelaez et al., 2012). These three crucial elements should therefore be taken into account when choosing a photocatalyst.

2.4.1 Various kinds of photocatalysts:

Titanium dioxide has been utilised as a photocatalyst in most photocatalytic dye degradation experiments; nevertheless, TiO_2's primary drawback is that, because of its 3.2 eV band gap, it can only absorb in the UV area (Viswanathan, 2017). Comparably, ZnO is a semiconductor with a band gap of 3.3 eV that is also frequently employed due to its wide availability and non-toxic nature; however, because of this wide band gap, its operational range is limited to the UV region (Zhao et al., 2014). Particularly TiO_2 and ZnO, semiconductors are used in thin porous films, nanorods, nanospheres, nanofibers, and nanowires, or they are supported on polymeric films (Meng & Juan, n.d.). Zinc oxide on a nanoscale is an inexpensive semiconductor with minimal environmental impact and low toxicity. Compared to TiO_2, it generates hydroxyl ions more effectively, producing emissions that are visible (Jana & Gregory, 2020). However, ZnO has several disadvantages, such as a high rate of electron-hole recombination (Anwer et al., 2019). However, TiO_2 and ZnO are not practicable for large-scale applications because of their broad band gap, fast charge recombination rates, and limited sensitivity to UV light (high hv), which makes up only 4-5 percent of the solar spectrum. This suggests that a narrow band gap photocatalyst sensitive to visible light (low hv), which makes up roughly 52% of the solar spectrum, is a better long-term option for reducing dye degradation. The flow diagram below shows the many types of photocatalysts and provides the following descriptions in Fig.10:

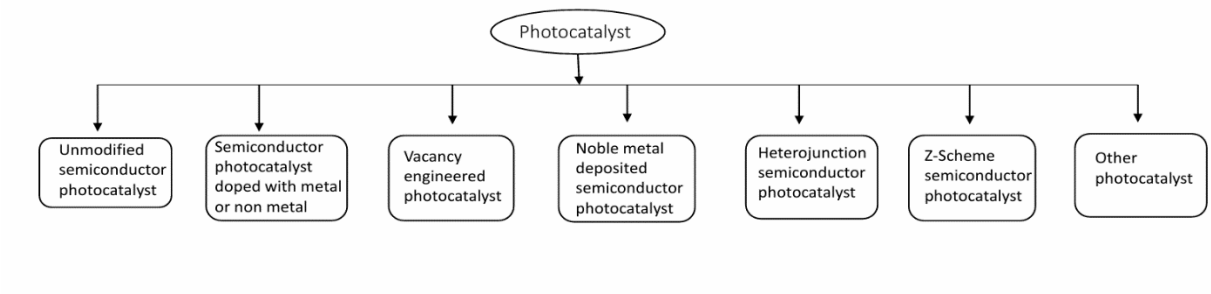

Fig.10: Various kinds of photocatalysts

(i) Semiconductor photocatalyst without modification:

A type of photocatalyst known as an unmodified semiconductor photocatalyst uses pure metal as a catalyst without altering its characteristics by the addition of other contaminants. Due to their ease of preparation, high chemical stability, and effective visible light response, metal-free narrow band gap (2.5–2.7 eV) semiconductors such as graphitic carbon nitride (g-C_3N_4), WO_3, BiOX (X = F, Br, Cl, and I), and others are commonly used as visible light photocatalysts. The production of $OH^{\bullet}$ is restricted by the photocatalyst's VB potential, which is less than the typical redox potentials of $OH^{\bullet}/H_2O$ and $OH^{\bullet}/OH^-$ (Hong, Li, et al., 2016). A single photocatalyst with strong redox activity and good visible light responsiveness is not achievable. The quick recombination of photogenerated e^-– h^+ couples is a significant drawback of pure, unmodified photocatalyst (Xue et al., 2015). Because of this, unaltered semiconductor photocatalysts are no longer typically utilised directly for the efficient removal of organic pollutants; instead, they are modified using a variety of techniques, such as doping, adding nanoparticles, producing vacancies, etc.

(ii) Metal-or non-metal-doped semiconductor photocatalyst:

By doping broad band-gap photocatalysts with metals (Sr, Co, Ti, Bi, Fe, etc.) and nonmetals (C, N, S, B, etc.), one can improve the efficiency of e^-–h^+ separation while simultaneously narrowing the band-gap and permitting visible light to flow through. TiO_2, ZnO, and g-C_3N_4 exhibit remarkable photocatalytic activity in the breakdown of organic pollutants; nevertheless, their broad band-gap renders them ineffective in the visible spectrum. ZnO nanoparticles were made more photocatalytically active throughout a broader range of wavelengths (UV to visible) by doping and adding impurities, which decreased the band gap energy of the particles (Sun et al., 2013). ZnO

nanoparticles have been altered with various dopants made of N and S atoms to improve the photocatalytic oxidation of organic dyes under UV and visible light irradiation (Shinde et al., 2012). When exposed to visible light, N-doped ZnO exhibited 96.22% efficiency in removing Methylene Blue (MB) dye (Prabakaran & Pillay, 2019). Similar to this, TiO_2/g-C_3N_4 heterojunction was found to have 90% efficiency in eliminating Methyl Orange (MO) dye when exposed to visible light. This efficiency rises to 99.8% when carbon, nitrogen, and sulphur heteroatoms are doped (Z. Huang et al., 2021b).

(iii) Photocatalyst with vacancy engineering:

The modification of photocatalyst characteristics is significantly influenced by defect engineering, specifically with regard to vacancies (Niu et al., 2018). According to Ding et al., vacancy induction enhances the electronic structure, prevents electron hole recombination, and can even function as a particular reaction site to increase photocatalytic activity. It helps to shorten the band-gap energy of the semiconductor, extending its range for light harvesting. Recent research has demonstrated that the production of nitrogen vacancies in g-C_3N_4 can greatly increase the bulk g-C_3N_4's photocatalytic efficiency ((Ding et al., 2018); (Niu et al., 2018); (Paquin et al., 2015)). Because it improves electron trapping and active sites—which in turn improve charge carrier separation, absorption, and activation ability for O_2 molecules—oxygen vacancy induced photocatalyst synthesis has recently gained attention as a research hotspot (Y. Huang et al., 2014). An oxygen vacancy-induced $BiO_{2-x}/Bi_2O_{2.75}$ Z-scheme heterojunction has been described by Wang et al. and has demonstrated enhanced photocatalytic activity (Wang et al., 2019). Goud and colleagues examined how surface oxygen vacancies promoted Z-scheme MoS_2/Bi_2O_3 heterojunction in relation to the elimination of Crystal Violet (CV) dye when exposed to visible light (Goud et al., 2020). Another work conducted by Khan et al. examined the impact of surface oxygen vacancy CeO_2-Graphene nanostructure on organic dye degradation (Khan et al., 2017).

(iv) Semiconductor photocatalyst deposited with noble metal:

Noble metals like Pt, Pd, Au, Ag, Cu, and others can be deposited on a semiconductor's surface to enhance its photocatalytic efficacy. In semiconductor–metal composites, photo-induced holes can stay on the semiconductor surface while photo-induced electrons in the conduction band (CB) can move to metal deposits, which function as electron acceptors, due

to the Schottky barrier at the metal–semiconductor heterojunction. Consequently, it is possible to prevent electron and hole recombination and boost photocatalytic effectiveness (Sá et al., 2008). When exposed to visible light, Pt deposited on TiO^2 demonstrated a high RhB removal efficiency (D. Zhang, 2012a). One of the best noble metals that is frequently utilised to increase semiconductor photocatalytic activity is silver. According to Mosavi et al., Ag-deposited CdSe/Zeolite nanocomposite removes MB dye with an approximate 90% efficiency when exposed to visible light (Mosavi et al., 2021). Ag/AgBr deposited Ag/Br/ZnO nanocomposite shown about 100% effectiveness for elimination of RhB dye under visible light irradiation, according to a different study by Shi et al. (Shi et al., 2014). Shen et al. (Shen et al., 2010) investigated the degradation potential of various noble metals, including Ag, Ru, Au, Pd, and Pt, and created a $CdS/M/TiO^2$ Z-scheme photocatalyst (M = Ag, Ru, Au, Pd, and Pt). They also observed the removal efficiency of MB dye under visible light irradiation.

(v) Semiconductor photocatalyst with heterojunction:

Nowadays, heterojunction photocatalysts are commonly employed because of their superior ability to separate photogenerated e^-–h^+ couples, which is a result of the synergistic benefits of each unique semiconductor. Heterojunction semiconductors combine two different semiconductor types—one n-type along with a p-type. One semiconductor's VB and CB are at a higher level than the other semiconductor in a type II heterojunction. A type II heterojunction can be formed by an n-type and p-type semiconductor, with the p-type having greater work function values and band edge levels than the n-type. At the heterojunction interface, there are positively charged n-type and negatively charged p-type semiconductors as a result of free e from the n-type semiconductor flowing to the p-type semiconductor after contact until equilibrium (EF) is established. An internal electric field is created as a result of band edge bending, and this causes a potential barrier to form. The e^--h^+ pair separation is caused by the internal electric field's facilitation of the transport of photogenerated e from the p-type CB to the n-type CB and photogenerated h^+ from the n-type VB to the p-type VB with incident light. Visible light can be strongly absorbed by copper sulphides (CuS), a p-type semiconductor with a small band gap of 2.0 eV. However, due to the quick recombination of the photo-induced e^-–h^+ pair, pure CuS has little photocatalytic activity (Gao et al., 2017b). Nanosheets of bismuth

tungstate (Bi_2WO_6) recombine easily with photogenerated carriers and exhibit a mild reaction to visible light. However, under visible light irradiation, the synthesis of Bi_2WO_6/CuS p-n heterojunction demonstrated around 99% efficacy towards the elimination of RhB (Mao et al., 2021). In a different illustration, we can see that zirconium oxide (ZrO_2), an n-type semiconductor with a large band gap of 5 eV, exhibits extremely low visible light efficiency. An n-type semiconductor with a comparatively small band gap of 2.7 eV is cerium oxide (CeO_2). Better photocatalytic properties were demonstrated by a combination of two semiconductors with varied and gap level energies of type n-n junction than by single ones.

(vi) Semiconductor photocatalyst with Z-scheme:

Z-schemes were inspired by the photosynthetic process of water splitting in nature (Natarajan et al., 2018b). The Z-scheme photocatalyst and a heterojunction share the same band structure configuration, but their charge carrier transfer mechanism is distinct. The Z-scheme may efficiently separate electrons and holes in various semiconductors while preserving larger oxidation and reduction potentials for holes and electrons compared to conventional Type I and Type heterojunctions (H. Li et al., 2015). For photocatalytic reactions, this exaction transfer mechanism separates and preserves photogenerated e^-–h^+ with better redox abilities spatially while promoting recombination of photogenerated e^-–h^+ with lower redox abilities (Q. Xu et al., 2018). Z-scheme systems can also be constructed with narrow band gap semiconductors, which increase the light absorption range while preserving the strong redox ability of the photocatalyst. Research on the creation of Z-scheme heterojunctions is promising since it can enhance the separation of charges and absorption of light (Wang et al., 2019). With a band-gap of 2.7 eV, bulk g-C_3N_4 is an excellent photocatalyst; nevertheless, its limited charge-transfer capacity usually limits the photocatalytic activity. Z-scheme heterojunctions can be produced to increase photocatalytic activity, but first it is important to find a semiconductor with the right band structure. The Z-scheme, which has a number of benefits including a narrow band gap, a wide range of light response, and reasonably stable chemical characteristics, can be created in this way using V_2O_5 semiconductor (Yan & Liu, 2020). The V_2O_5/g-C_3N_4 Z-scheme heterojunction composite was created by Hong, Jiang, et al. using thermal polymerization. They discovered that this composite's efficiency in

photocatalytic degradations of Rhodamine B (RhB) was much higher than that of V_2O_5 and g-C_3N_4 (Hong et al., 2016).

(vii) Alternative Photocatalyst:

Currently, nanocomposite photocatalysts, which are essentially combinations of several photocatalysts, are primarily in use. Although these nanocomposites do not fit into any of the previously listed categories, we can still learn something about their charge transfer mechanism from them. When exposed to visible light, these nanocomposites are incredibly effective at degrading synthetic dyes. Ag-based semiconductors, for instance, AgX (X = Cl, Br, I), Ag_2CrO_4, Ag_2MoO_4, $AgVO_3$, Ag_3PO_4, Ag_2CO_3, Ag_2WO_4, etc., are interesting candidates for photocatalysis because of their narrow band-gap, which allows them to respond to visible light efficiently. Among these is the Ag_2MoO_4 nanoparticle, which is widely employed in many different applications, including ion-conducting glasses, gas sensing, photo-switch devices, and antimicrobial agents ((Deb & Ghosh, 2011); (Gouveia et al., 2014)). According to Zhang et al. (2021) Bi_2MoO_6 is a less active photocatalytic agent in the visible spectrum but a great one in the ultraviolet (Z. Zhang et al., 2021). In order to remove MB dye under visible light, Balasurya et al. produced a Bi_2MoO_6/Ag_2MoO_4 nanocomposite that exhibits 91.8% efficiency (Balasurya et al., 2021). For instance, copper selenide (CuSe), a p type semiconducting material with a greater surface area, superior electrical and optical properties, and a wider band gap, is less efficient when exposed to visible light. CuSe and Graphene Oxide (GO) (CuSe/GO composite) reduce electron-hole pair recombination due to GO's superior electron conduction ability, which raises the photocatalytic activity of the semiconductor materials (Ata et al., 2018). CuSe/GO nanocomposite was developed by Iqbal et al., who reported 89% efficacy in MG dye removal under visible light (Iqbal et al., 2021). Similarly, two newly found nanocomposites that demonstrate excellent efficiency towards the elimination of MB dye under visible light irradiation are BPN & ZnAl-LDH nanocomposite (Yang et al., 2021) and TiO_2/PVA(Polyvinyl Alcohol)/cork nanocomposite (Mohamad Idris et al., 2021a).

2.4.2 Dye degradation by photocatalysis:

As previously mentioned, conventional treatment methods such as chemical coagulation, electrocoagulation, biological process, adsorption, etc., cannot entirely eliminate the dyes. These procedures also have a number of drawbacks, such as high costs, the formation of sludge, difficulty handling, etc. To remove these dyes, an advanced oxidation method is employed. One of the more advanced oxidation techniques that effectively removes dye is photocatalysis. The basic mechanism of photocatalysis has already been covered. Numerous forms of photocatalysis exist, including unaltered photocatalysis, photocatalysis with Nobel metal deposited on it, vacancy engineered photocatalysis, heterostructure photocatalysis, and z scheme photocatalysis, which were previously covered in the previous chapter. The most popular semiconductor photocatalysts for treating pollution are TiO_2, ZnO, WO_3, and so on; however, because of their large band gaps, these photocatalysts are unable to remove dyes in the visible range. Because of this, scholars are primarily concerned with creation of a nanocomposite, which combines a semiconductor photocatalyst with a variety of materials to provide excellent removal efficiency. The following is a chronological description of the various literatures and contemporary developments on photocatalysis removal of dye under visible light irradiation.

In order to remove MB under visible light irradiation, X. Liu et al. effectively synthesised a novel bi-functional Z-scheme heterojunction WO_3/g-C_3N_4 with a well-defined morphology using an in-situ liquid phase technique. In 90 minutes, it has a 95% clearance efficiency. Based on the active species trapping tests, a Z-scheme heterojunction system generation may be the mechanism for the potential improvement of photocatalytic activity. According to observations, O_2 is the primary reactive species that breaks down MB (Liu et al., 2017).

Ag/AgBr/ZnO composites were created by Shi et al. by a two-step deposition precipitation process, which was followed by reduction under visible light irradiation to eliminate the RhB dye. Ag/AgBr/ZnO composites outperformed pure ZnO in photocatalytic activity for RhB dye degradation when exposed to visible light. The enhanced photocatalytic activity is assumed to be caused by synergistic effects, including enhanced visible light absorption, a reduced band gap, and effective separation of photogenerated electron-hole pairs. Additionally, after 10 cycles, catalytic repeated testing showed that the Ag/AgBr/ZnO composite retained good stability, with activity marginally declining (Shi et al., 2014).

Dongfang Zhang used a soft chemical reduction technique to create metallic platinum Pt/TiO_2 nanocomposites and titania nanoparticles that may be used to remove RhB when exposed to visible light. The Pt/TiO_2 nanocomposite photocatalyst's superior visible light-driven photocatalytic activity is responsible for the high efficiency of charge-pair separation caused by the presence of deposited Pt serving as electron sinks to retard the rapid $e^{-}h^{+}$ couple recombination, the good photo absorption capacity in the visible light region, and the higher concentration of surface hydroxyl groups, which can effectively scavenge photogenerated valence band holes. As holes build up on the catalyst surface, more $OH^{\bullet}$ is formed, a reactive species that quickly oxidises the organic dye molecule (D. Zhang, 2012b).

The photocatalytic breakdown of MB over titania-doped copper ferrite, or $CuFe_2O_4/TiO_2$ photocatalyst synthesised via sol-gel technique under visible light irradiation, was reported by Arifin et al. At the ideal dose of 0.5 g/L, it demonstrated a maximum efficiency of 83.7% after three hours of radiation exposure. By effectively separating charges, this photocatalyst increases photocatalytic activity by facilitating photon absorption and reducing electron-hole pair recombination (Arifin et al., 2019).

Nitrogen doped zinc oxide nanoparticles with a cabbage-like morphology (N-ZnONCBs) were created by Prabakaran and Pillay using a hydrothermal technique, and they were used as a photocatalyst for the photocatalytic degradation of MB in the presence of UV and visible light. Upon exposure to 80 minutes of UV light and 50 minutes of visible light, respectively, the N-ZnONCB photocatalyst demonstrated effective MB degradation (98.6 percent and 96.2 percent). The dye in this experiment was fully calcified. The N-ZnONCB catalyst's photo-stability and reusability were also examined; following four cycles, the degradation rate was MB (93.2%). It has been demonstrated that the radicals $^{\bullet}O_2^{-}$ and $OH^{\bullet}$ are both effective oxidising agents that quickly react with the MB molecule to yield the breakdown products CO_2, H_2O, Cl, SO_4^{2-}, and NO_3^{-} (Prabakaran & Pillay, 2019).

Reduced graphene oxide-zinc oxide (rGO-ZnO) composite was made by Ferreira et al. using a one-step procedure to remove MB when exposed to visible light. In ninety minutes, the removal efficiency is 98%. The composite is very useful for water purification applications because of the photocatalytic qualities of ZnO and the effective adsorption capacity of rGO sheets (Ferreira et al., 2020).

Ghosh and Pal described the straightforward creation of a novel visible light active photocatalyst by hydrothermally loading Bi_2O_3 nanoparticles on nitrogen-vacant 2D g-C_3N_4 nanosheets for the removal of MB in the presence of LED light. This led to an increase in the efficiency of electron hole separation and an increase in photocatalytic activity for MB breakdown. In 60 minutes, it demonstrates a 92% eradication efficiency (Ghosh & Pal, 2020a).

El-Katori et al. synthesized a CdS/SnO_2 heterostructure that is both recyclable and effective for photocatalytically degrading MB dye in the presence of UV and ambient light. This photocatalyst prolonged the life of the reactive radicals and improved the charge carrier's separation efficiency. Superoxide radicals and conduction band electrons have been found to be the main reactive species for photocatalytic activity. (El-Katori et al., 2020) report that the catalyst demonstrates exceptional photocatalytic stability, as evidenced by its capacity to preserve 83% of its reactivity even after five successive cycles, indicating no structural damage.

In order to remove MB under visible light irradiation, Lei et al. generated Fe_3O_4@ZnO-RGO (RGO: reduced graphene oxide) composite with magnetic separation using the low-temperature hydrothermal method. Fe_3O_4@ZnO RGO has good photocatalytic activity, cyclic stability, and a larger MB adsorption range in visible light when compared to pure ZnO and Fe_3O_4@ZnO nanoparticles. Additionally, Fe_3O_4@ZnO-RGO's distinct structural features allowed electron-hole pairs to separate, which improved the material's photocatalytic capabilities (Lei et al., 2020).

Chaudhary and colleagues synthesised new graphene-supported ternary nanocomposites (WO_3-ZnO@rGO) by utilising easy ultrasonic assisted WO_3-ZnO binary nanostructure creation over 2D rGO nanosheets for the elimination of MB under visible light irradiation. When WO_3-ZnO was impregnated over rGO sheets, the photocatalytic effectiveness of WO_3-ZnO@rGO was dramatically increased. Within 90 minutes, 94 percent of the dye was removed under visible light irradiation. Through efficient separation and transmission of photo-induced electron-hole pairs, the photocatalytic efficiency was enhanced by the WO_3-ZnO@rGO. Furthermore, WO_3-ZnO@rGO continued to exhibit outstanding dye degradation efficiency even after four recycling tests. Additionally, it has been found that ROS contribute to the MB degradation in the following order: $OH^{\bullet} > h^{+} > {}^{\bullet}O_2^{-}$ (Chaudhary et al., 2020).

Mosavi et al. used Response Surface Methodology (RSM) to construct Ag@CdSe/Zeoilte photocatalyst and investigated its ability to remove MB dye. Their results showed that 89.98 percent of the MB was removed at [MB] = 7.17 mg/L, Ag@CdSe/Zeolite dose = 0.03 g/50 mL, pH = 8, and t = 40 minutes. Additionally, they noticed that MB easily combines with $OH^{\bullet}$ in an alkaline medium to produce CO_2 gas, which is then efficiently eliminated from the mixture (Mosavi et al., 2021).

Y. Zhang et al. used a simple hydrothermal process to create a 2D/2D Z-scheme heterostructure photocatalyst of BiOBr/TzDa covalent organic framework (COF) (BTDC) for the elimination of RhB/Cr(VI) combination. In 20 minutes and 40 minutes, respectively, about 97% of the entire RhB and Cr(VI) in the mixture could be eliminated. They find that h^+ and $^{\bullet}O_2$ are essential to the breakdown of RhB, but $OH^{\bullet}$ is not as Important. They also find that the reactive species that cause RhB degradation function less effectively in the order of $h^+ > {}^{\bullet}O_2^- > OH^{\bullet}$ (Y. Zhang et al., 2021).

Zhang X. et al. conducted an analysis on the removal of MO dye from water using a heterojunction photocatalyst with the Z-scheme V_2O_5/P-g-C_3N_4 under visible light irradiation. The findings demonstrated that MO was degraded at the fastest apparent rate by the V_2O_5/P-g-C_3N_4 Z-scheme heterostructure, which did so 14.5 and 3.7 times quicker than V_2O_5 and P-g-C_3N_4 when utilised independently. They were able to reach 90% efficiency in just 105 minutes. Additionally, they found that h^+ and $^{\bullet}O_2^-$ were the main active species in the photocatalytic degradation of MO (X. Zhang et al., 2021).

Carbon-nitrogen-sulfur co-doped TiO_2/g C_3N_4 Z-scheme heterojunction photocatalyst, synthesised by one-step hydrothermal and calcinations procedures under visible light irradiation, was examined by Z. Huang et al. for its ability to remove MO dye. When compared to pure TiO_2 and g-C_3N_4, the CNS- TiO_2/g-C_3N_4 Z-scheme heterojunction photocatalyst shown outstanding degrading performance (99.8%) under visible light irradiation. They have found that h^+ has a negligible impact on the MO photocatalytic degradation process, whereas $^{\bullet}O_2^-$ & $OH^{\bullet}$ play an active role (Z. Huang et al., 2021a).

When exposed to visible light, Ghattavi & Nezamzadeh-Ejhieh built a double Z-scheme AgI/ZnO/WO_3 photocatalyst for the removal of MB. Reduced electron/hole recombination in this photocatalyst is favourable to the photocatalytic activity. In 48.5 minutes, 85.2% of MB is eliminated. According to research, the composite's most important contributions to the photodegradation of MB are the hydroxyl radicals and photogenerated holes (Ghattavi & Nezamzadeh-Ejhieh, 2021).

In order to remove MB under visible light irradiation, Yang et al. developed a novel type of environmentally friendly nanocomposite made of ZnAl layered double hydroxides (LDH) and black phosphorus nanosheets (BPNs), which were produced by electrostatic self-assembly approach. In 80 minutes, the ZnAl LDH and BPNs nanocomposite photocatalyst demonstrates 99% MB degradation. The fundamental reason for the increase in photocatalytic performance is that BPNs offer an extra electron and hole transport channel. While $^{\bullet}O_2^-$ is not the primary species, it is further transformed to $OH^{\bullet}$ by reductive pathways ($^{\bullet}O_2^- \rightarrow H_2O_2 \rightarrow OH^{\bullet}$), which are primarily responsible for the breakdown of MB (Yang et al., 2021).

The titanium dioxide nanoparticles (TiO_2 NPs) / polyvinyl alcohol (PVA) / cork nanocomposite was described by Mohammed Idris et al. as a floating photocatalyst. The cork acts as a floating substrate, and TiO_2 NPs are anchored on the surface of the cork by using polyvinyl alcohol (PVA) as a binder. This photocatalyst was employed to remove MB when exposed to visible light. Compared to anatase TiO_2, this nanocomposite was shown to have a reduced rate of electron-hole pair recombination. Under a visible light source, the TiO_2/PVA/cork floating photocatalyst deteriorated at 98.43% of Methylene Blue (MB) after 120 minutes at the ideal mole ratio of 1:8. The superoxide radical's reactive oxygen species ($^{\bullet}O_2^-$) primarily regulated MB's superior photodegradation performance. According to (Mohamad Idris et al., 2021b) the degradation kinetics of MB were first-order kinetics.

Asadzadeh-Khaneghah and colleagues created g-C_3N_4 nanosheet/carbon dot/FeOCl (also referred to as C_3N_4 NS/CD/FeOCl) nano-composites using a straightforward calcinations process to photodegrade RhB dyes when exposed to visible light. The results showed that 0.1 g of the ideal nanocomposite could effectively remove 250 mL of RhB solution in 60 minutes. They note that the elimination reaction is aided by h^+, $OH^{\bullet}$, and O_2^- (Asadzadeh-Khaneghah et al., 2021).

Using the auto solution combustion approach, Noman et al. synthesised p-n CuO/CeO_2ZrO_2 heterojunction photocatalyst for the elimination of Methylene Blue (MB) dye under visible light irradiation. This indicates a 3 hour elimination efficiency of 98%. They found that the primary players in the photocatalytic degradation process are $OH^{\bullet}$, O_2^-, and h^+. Conversely, CuO/CeO_2ZrO_2's degradation of MB was unaffected by H_2O_2 (Aiman M.A Noman et al., 2021).

Balasurya et al. investigated the elimination of Methylene Blue (MB) dye under visible light irradiation using a Bi_2MoO_6-Ag_2MoO_4 nanocomposite heterojunction photocatalyst synthesised by a simple synthesis process. After the sixth cycle, the Bi_2MoO_6-Ag_2MoO_4 nanocomposite showed 91.8% degrading efficiency, which was much better than the individual values of Ag_2MoO_4 (54.66%) and Bi_2MoO_6 (58.6%). They further claim that this heterojunction can speed up the photocatalytic degradation process and stop the e^-/h^+ pair from recombining. According to Balasurya et al. (2021) $OH^\bullet$ is mostly responsible for the photocatalytic breakdown of MB dye (Balasurya et al., 2021).

To remove Rhodamine B (RhB) dye under visible light irradiation, Mao et al. synthesised a Bi_2WO_6/CuS p-n heterojunction photocatalyst. In 105 minutes, around 98.8% of the RhB (10 mg/L) in a mixed solution was eliminated. Here, photogenerated electrons and holes moved to the Bi_2WO_6/CuS surface, where they immediately removed the RhB. Bi_2WO_6/CuS has significant photocatalytic activity and can be used to remove RhB over a wide pH range of 2–6 (Mao et al., 2021).

In order to remove methyl green under solar light irradiation, Iqbal et al. examined the photocatalytic activity of a composite of copper selenide nanoparticles and graphene oxide (CuSe/GO). A CuSe/GO composite was created by utilising a modified Hummer's method for GO and a hydrothermal method for CuSe. CuSe/GO eliminated 89 percent of the MG in 45 minutes (Iqbal et al., 2021).

Chapter: 3

3. MATERIALS AND METHODS

3.1 MATERIALS:

The synthetic Merck MB solution is made and utilised as an organic contaminant. The materials used to synthesise Bi_4NbO_8Cl are Bismuth oxychloride (BiOCl: 98% extra pure), Niobium pentoxide (Nb_2O_5: 99.9%), and Bismuth Oxide (Bi_2O_3: 99% extra pure), all from Loba Cheme. As molten salt, sodium chloride (NaCl: Merck) and potassium chloride (KCl: Basynth) are utilised. g-C_3N_4 was synthesised using Merck's urea ($CO(NH_2)_2$). The entire study was conducted using Millipore water.

3.2 PHOTOCATALYST SYNTHESIS:

3.2.1 SYNTHESIS OF g-C_3N_4 (UGCN) NANOSHEETS:

In compliance with previous study, thermal poly-condensation of urea was used to synthesise the g-C_3N_4 nanosheets (henceforth referred to as UGCN). Generally, a covered alumina crucible was placed inside a muffle furnace and 25g of urea was calcined for 4 hours at 550 °C. After grinding, the product was calcined again for two hours at 500 °C. After that, the resultant yellowish powder was grinding and kept it for further use (Majumdar et al., 2021).

3.2.2 SYNTHESIS OF Bi_4NbO_8Cl (BNOC) NANOSHEETS:

Bi_2O_3 (Loba Cheme Pvt Ltd., 99%; 3.21gm), BiOCl (Loba Cheme Pvt Ltd., 98%; 1.19gm), and Nb_2O_5 (Loba Cheme Pvt Ltd., 99.9%; 0.6gm) were the raw materials used in the flux process used to synthesis the Bi_4NbO_8Cl samples. Use of a molten alkali metal chloride salt as a flux included NaCl (Merk; 1.1187gm), KCl (Basynth; 1.808gm), or the eutectic mixture (1: 1.267). At a solute concentration of 5 mol%, the flow was combined with Bi_2O_3, BiOCl, and Nb_2O_5 at the stoichiometric molar ratio for Bi_4NbO_8Cl (3:2:1). The mixture was put in an alumina crucible with cover and heated in a muffle furnace to 700 °C, maintaining the temperature for 10 hours. The heating rate was set at 50 °C per hour. The Bi_4NbO_8Cl was thoroughly cleaned with Millipore water once it had cooled to room temperature. After a 24 hour drying process at 80 °C, it was kept for further use (Ogawa et al., 2019a).

3.2.3. SYNTHESIS OF g-C_3N_4/Bi_4NbO_8Cl NANOCOMPOSITE:

Utilising the hydrothermal technique, the Bi_4NbO_8Cl/ g-C_3N_4 nanocomposite was created. First, 40 millilitres of deionized water were mixed with 100 mg of Bi_4NbO_8Cl and a predetermined quantity of g-C_3N_4 nanosheets. This was followed by 30 minutes of sonication. Next, 40 millilitres of deionized water were mixed with 100 mg of g-C_3N_4 nanosheets and a predetermined amount of Bi_4NbO_8Cl. Following that, the mixes were put in a 50 mL hydrothermal autoclave lined with Teflon and heated to 160°C for 24 hours. After the hydrothermal treatment, the products were thoroughly washed and dried at 80°C for a whole day. Figure No. 11 below shows the Bi_4NbO_8Cl/g-C_3N_4 nanocomposites synthesis technique. g-C_3N_4/Bi_4NbO_8Cl nanocomposites with mass ratios of 10, 20, 30, and 40% were obtained by varying the amount of g-C_3N_4 nanosheets. These nanocomposites are referred to as 10g-C_3N_4/ Bi_4NbO_8Cl, 20 g-C_3N_4/Bi_4NbO_8Cl, 30g-C_3N_4/Bi_4NbO_8Cl, and 40g-C_3N_4/ Bi_4NbO_8Cl. Different amounts of Bi_4NbO_8Cl nanosheets were used to create Bi_4NbO_8Cl/g-C_3N_4 nanocomposites with mass ratios of 10, 20, 30, 40, 50, and 60%. These are referred to as 10Bi_4NbO_8Cl/g-C_3N_4, 20Bi_4NbO_8Cl/g-C_3N_4, 30Bi_4NbO_8Cl/g-C_3N_4, 40Bi_4NbO_8Cl/g-C_3N_4, 50Bi_4NbO_8Cl/g-C_3N_4, and 60Bi_4NbO_8Cl/g-C_3N_4, respectively. Below is Figure 11, which depicts the schematic diagram used to create Bi_4NbO_8Cl.

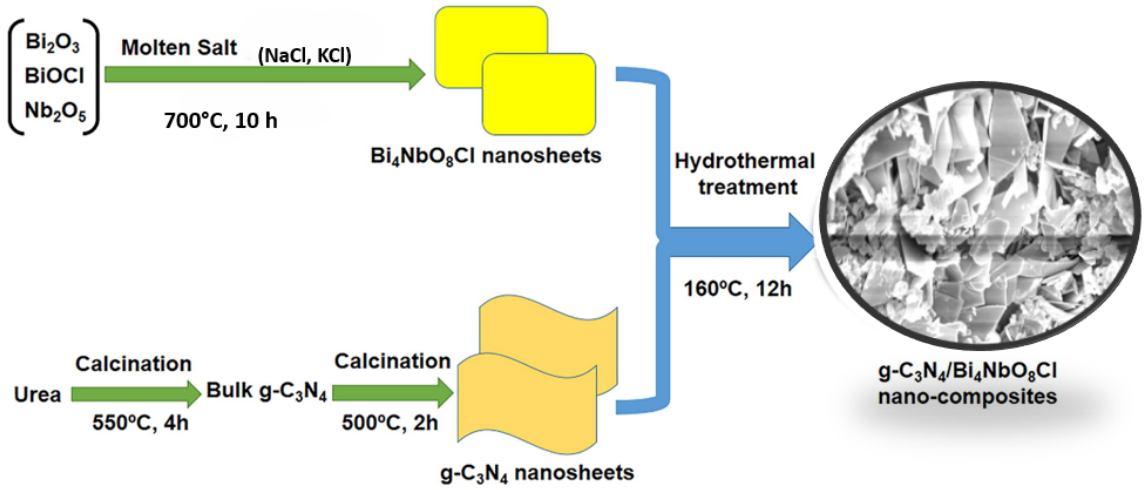

Fig.11. Synthesis of g-C_3N_4/Bi_4NbO_8Cl Nanocomposite

3.3 CHARACTERIZATION:

Morphological observations and EDX (Energy Dispersive X-ray Spectroscopy) analysis were conducted using a Zeiss MERLIN scanning electron microscope (SEM). The XRD pattern was obtained using an X-ray diffractometer (Model: PANalytical, X'Pert³ Powder). The optical characteristics were assessed using a PerkinElmer UV/Vis Spectrophotometer Lambda 25.

3.4 PHOTOCATALYTIC EXPERIMENT:

In order to determine the photocatalytic efficiency of the as-synthesised Bi_4NbO_8Cl/g-C_3N_4 nano-composites, MB was degraded under the influence of a visible LED light (20-W, Philips, India). The light's measured intensity was 10 mW cm^2. Generally, 10mL of MB (10 mgL^{-1}) was added to a glass beaker along with a 10 mg dosage of the photocatalyst. An adsorption–desorption equilibrium between the catalyst and MB was achieved by agitating the mixture with a magnetic stirrer at 500 rpm for 40 minutes while it was dark. The photocatalytic reaction under light irradiation came next for 60 minutes. Following the photocatalytic reaction's conclusion, the supernatant was filtered using a 0.22 mm syringe filter and tested for MB at a wavelength of 664 nm using an PerkinElmer UV/Vis Spectrophotometer Lambda 25. Equation (1) was used to calculate the MB removal.

$$\text{MB degradation (\%)} = \frac{C_0 - C}{C_0} \times 100 \qquad \ldots. (1)$$

where C_0 and C are the initial and final concentrations of MB, respectively

3.5 RADICAL SCAVENGING EXPERIMENT:

The scavenging of superoxide radicals ($^{\bullet}O_2$), holes (h^+), and hydroxyl radicals ($^{\bullet}OH$) was accomplished by using radical scavengers such as benzoquinone (BQ), ethylenediamine tetraacetic acid disodium salt (EDTA-2Na), and isopropanol (IPA). The concentrations of the BQ, EDTA-2Na, and IPA were 0.25 mM, 1 mM, and 1 mM, respectively. Similar photocatalytic degradation tests were carried out, but this time scavengers were added to the solutions beforehand.

Chapter:4

4. RESULTS AND DISCUSSION:

4.1. X-ray DIFFRACTION ANALYSIS (XRD):

Fig. 12 shows the crystal lattice structure and XRD patterns of the synthesised catalysts that could be found using XRD analysis. The orthorhombic phase of Bi_4NbO_8Cl (JCPDS No. 84-0843) and the XRD pattern of the nanosheets were identical. The characteristic peak of g-C_3N_4, which corresponds to the interlayer stacking of graphitic sheets, is the strong diffraction peak of g-C_3N_4 nanosheets around 27.45° (Ghosh & Pal, 2020b). The peaks belonging to both g-C_3N_4 and Bi_4NbO_8Cl made up the patterns of g-C_3N_4/Bi_4NbO_8Cl nano-composites. This suggests that g-C_3N_4 and Bi_4NbO_8Cl nanosheets were fused together with a strong interfacial contact after hydrothermal treatment.

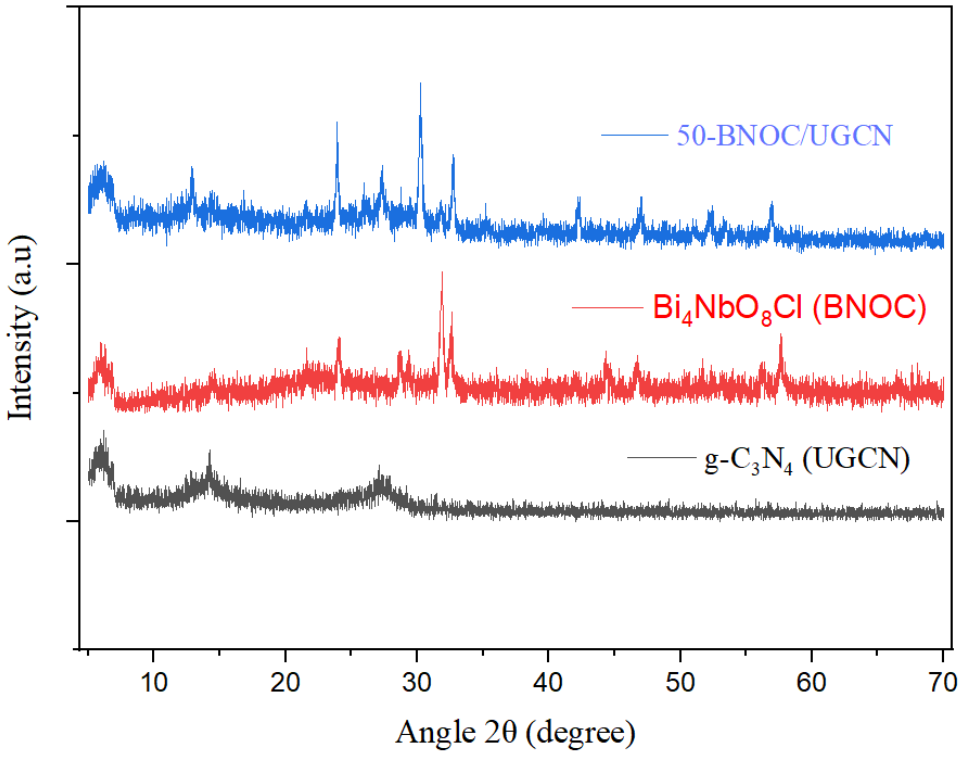

Fig. 12. XRD patterns of g-C_3N_4, Bi_4NbO_8Cl, and 50-BNOC/UGCN nano-composites

4.2. FESEM:

Using a FESEM analysis, the detailed morphology of g-C_3N_4 nanosheets, Bi_4NbO_8Cl nanosheets, and the 50-Bi_4NbO_8Cl/g-C_3N_4 nano-composite was examined and is shown in Fig. 13-15. The FESEM picture of Bi_4NbO_8Cl (Fig. 13) verified the nanosheet-like morphology of the material, which was generated by flux synthesis and has a thickness ranging from 56 to 66 nm. Bi_4NbO_8Cl has a similar shape, according to a prior work (Ogawa et al., 2019b). The picture in Fig. 14 made the formation of g-C_3N_4 nanosheets clear. It is evident from the 50-Bi_4NbO_8Cl/g-C_3N_4 image (Fig. 15) that following the hydrothermal treatment, the Bi_4NbO_8Cl nanosheets were uniformly deposited on the surface of the g-C_3N_4 nanosheets.

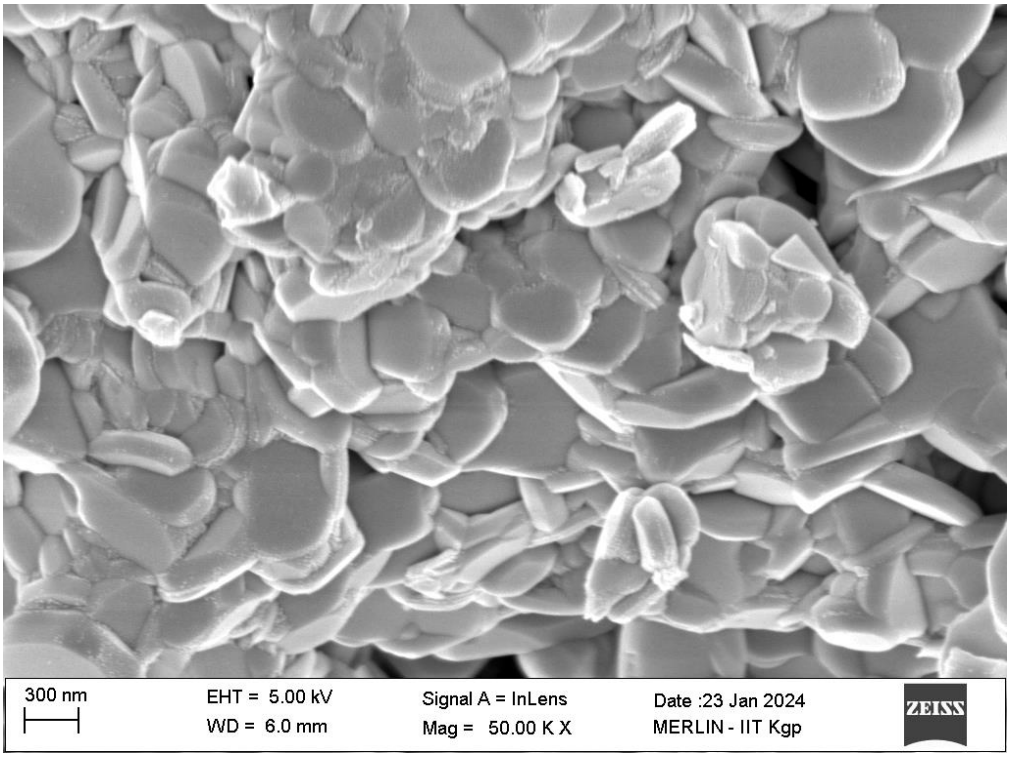

Fig. 13. FESEM images of Bi_4NbO_8Cl nanosheets

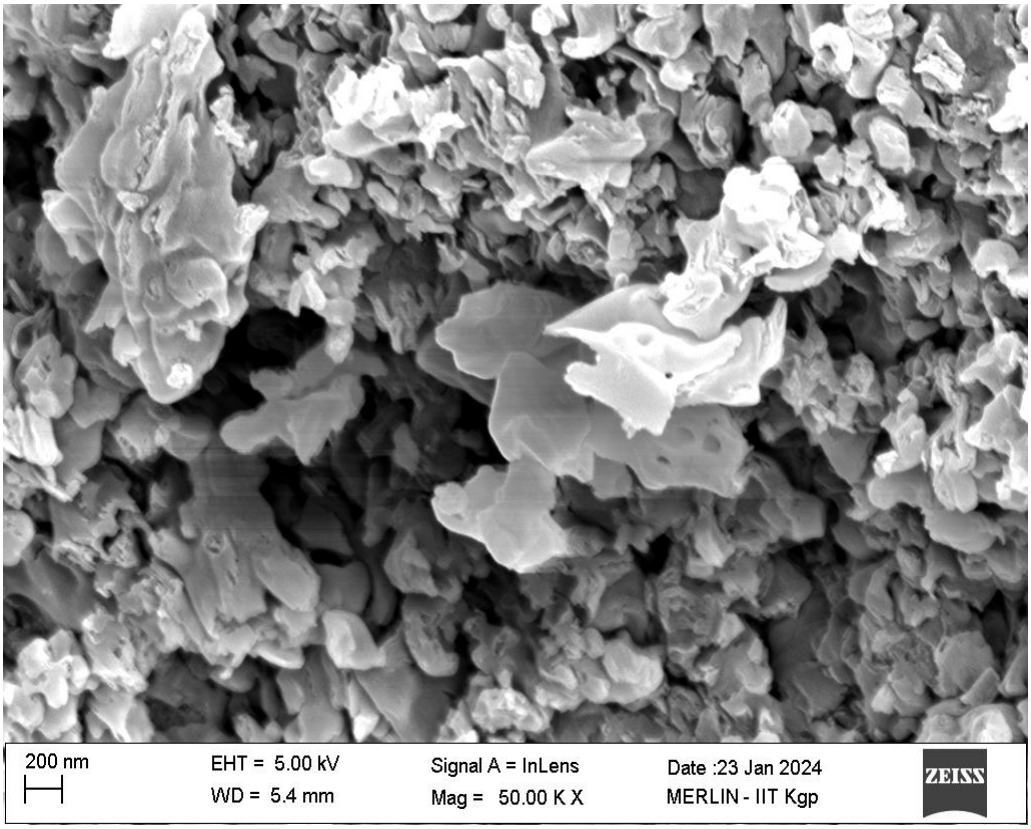

Fig. 14. FESEM images of g-C_3N_4 nanosheets.

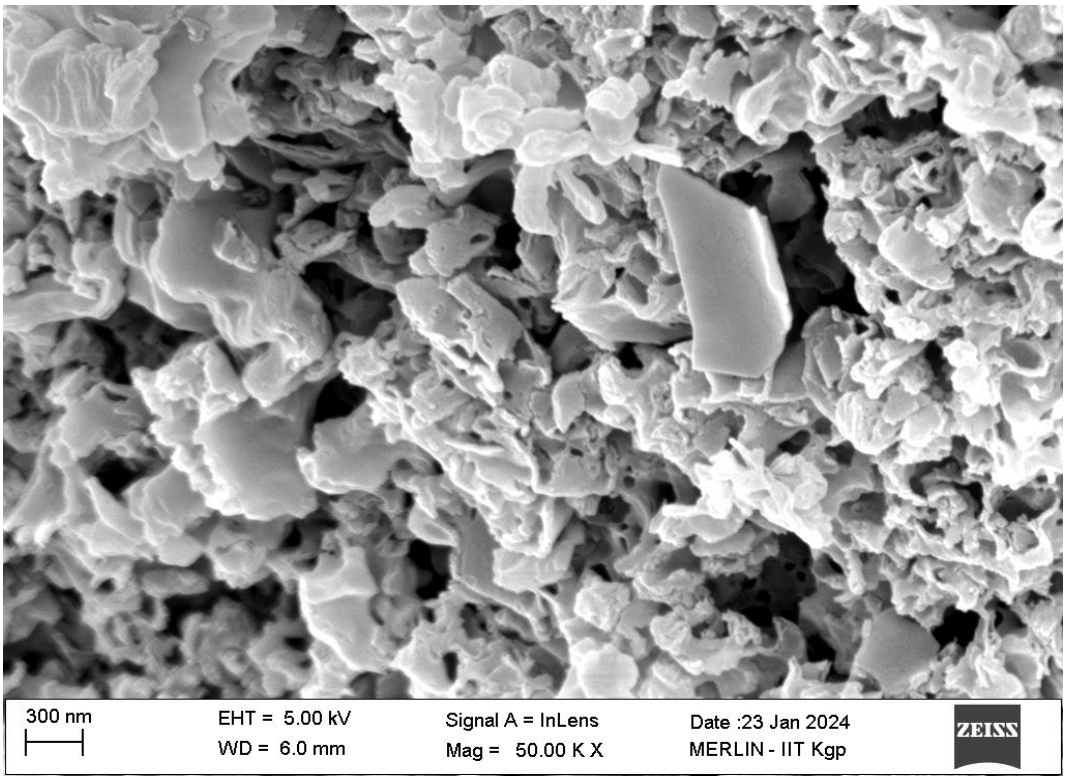

Fig. 15. FESEM images of 50-Bi_4NbO_8Cl/g-C_3N_4 nanocomposite

4.3 EDX MAPPING:

The energy-dispersive X-ray (EDX) spectrum confirms the presence of C and N, in the synthesized g-C_3N_4 nanosheet (Fig. 16). The energy-dispersive X-ray (EDX) spectrum confirms the presence of Bi, Nb, O and Cl, in the synthesized Bi_4NbO_8Cl nanosheet (Fig. 17). The energy-dispersive X-ray (EDX) spectrum confirms the presence of Bi, Nb, O, Cl, C and N, in the synthesized 50-Bi_4NbO_8Cl/g-C_3N_4 nano-composite (Fig. 18).

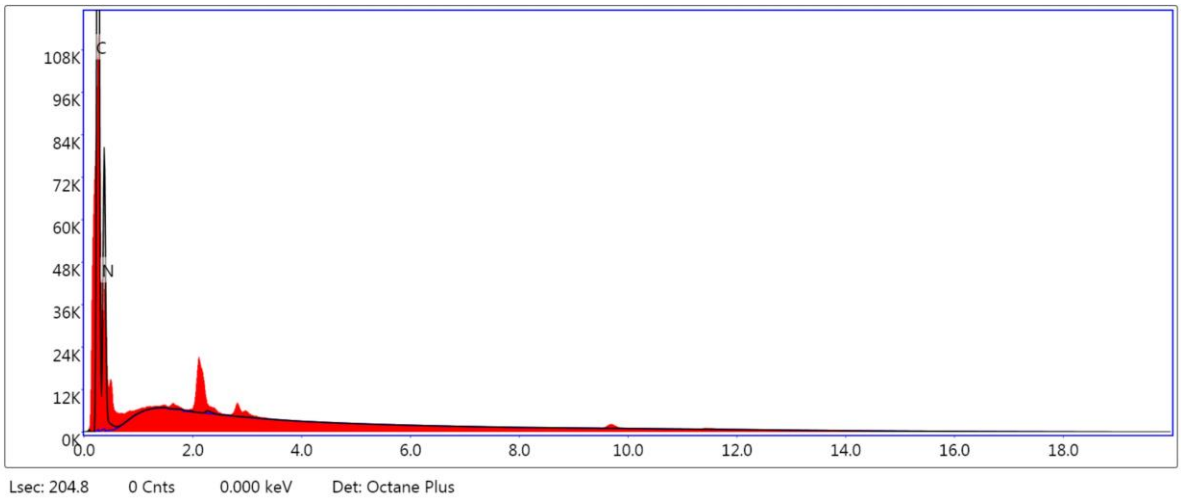

Fig. 16. EDX of g-C_3N_4 nanosheet

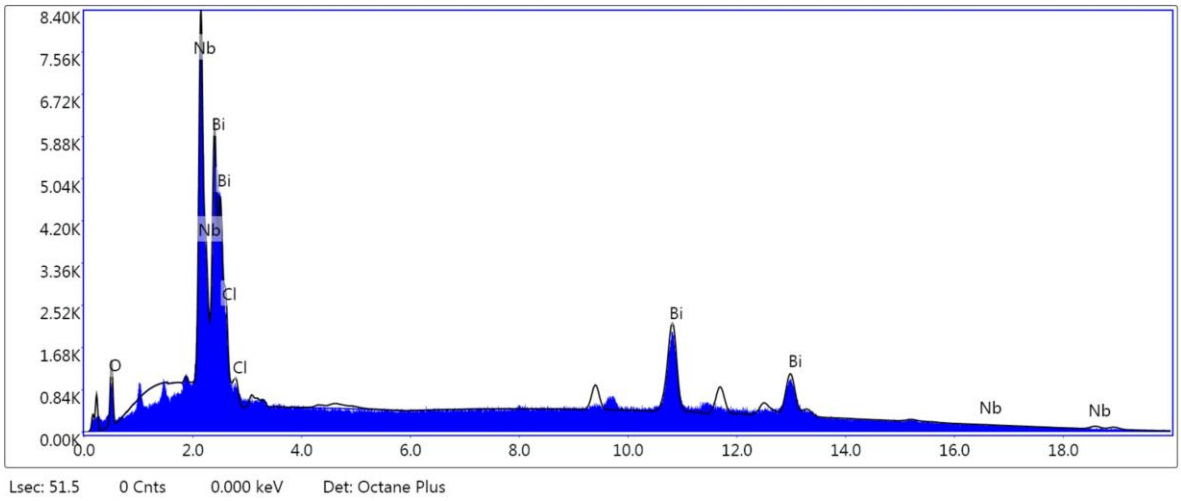

Fig. 17. EDX of Bi_4NbO_8Cl nanosheet

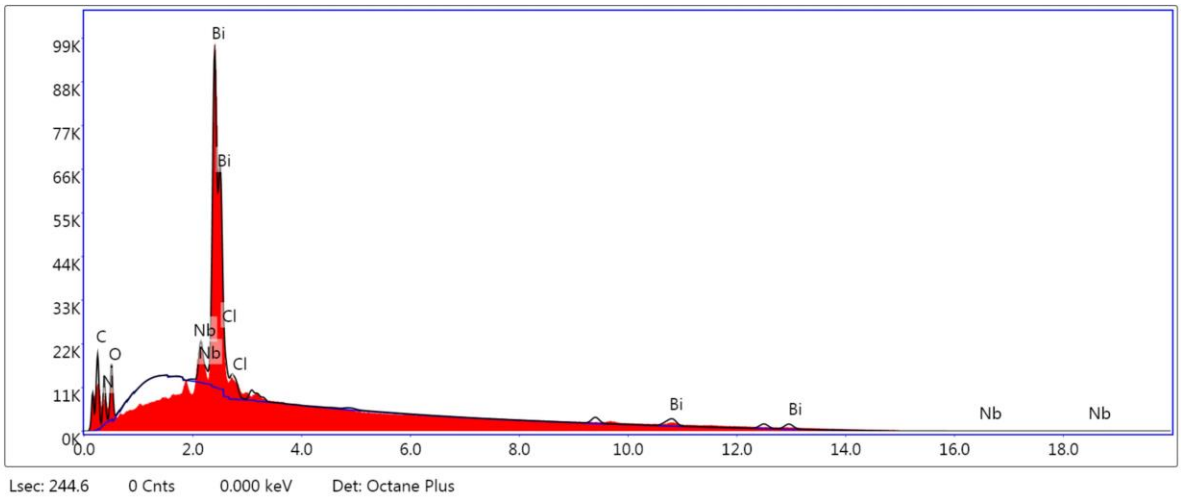

Fig. 18. EDX of 50-Bi_4NbO_8Cl/g-C_3N_4 nano-composite

4.4 UV-visible DRS:

The performance of a photocatalyst is greatly influenced by its optical characteristics. In Figs. 19, 20 and 21, respectively, the UV-visible DRS of the nano-composites Bi_4NbO_8Cl, g-C_3N_4 and 50-Bi_4NbO_8Cl/g-C_3N_4 are displayed. The g-C_3N_4 and Bi_4NbO_8Cl nanosheets' absorption edges are situated at about 440 and 520 nm, respectively (Majumdar et al., 2021). From the bandgap energies (Eg) of 50-Bi_4NbO_8Cl/g-C_3N_4, Bi_4NbO_8Cl, and g-C_3N_4 were found to be 2.60 eV, 2.61 eV, and 3.04 eV, in that order. It is possible to attribute the increased absorption in the visible light range and consequently higher photocatalytic efficiency of 50-Bi_4NbO_8Cl / g-C_3N_4 to the complementary effects of g-C_3N_4 and Bi_4NbO_8Cl nanosheets. According to estimates derived from Mott-Schottky plots in earlier research, the conduction band (CB) potential values of g-C_3N_4 (vs. NHE) and Bi_4NbO_8Cl were 1.2 eV and 0.54 eV (Majumdar et al., 2021), respectively. Bi_4NbO_8Cl and g-C_3N_4's valence band (VB) potential was determined using Eq. (9),

$$E_{VB} = E_g + E_{CB} \quad \text{..... (9)}$$

where VB and CB potential are denoted, respectively, by E_{VB} and E_{CB}. As a result, +2.07 eV and +1.84 eV, respectively, are the estimated valence band (VB) potential values of Bi_4NbO_8Cl and g-C_3N_4.

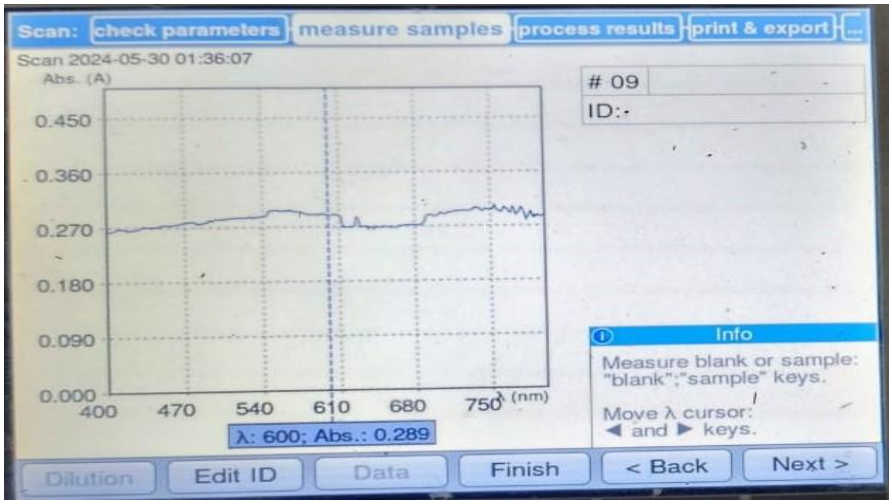

Fig. 19. UV-vis DRS for Bi_4NbO_8Cl

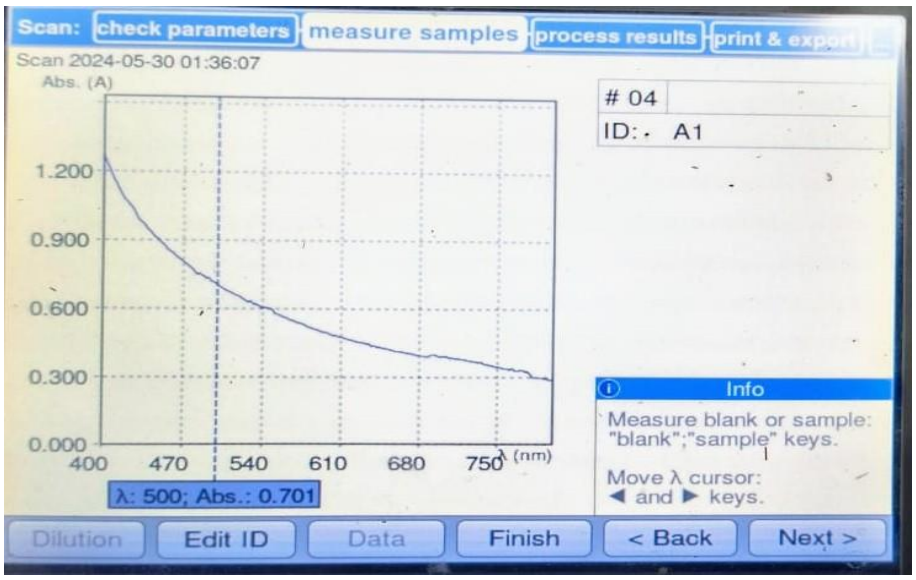

Fig. 20. UV-vis DRS for g-C_3N_4

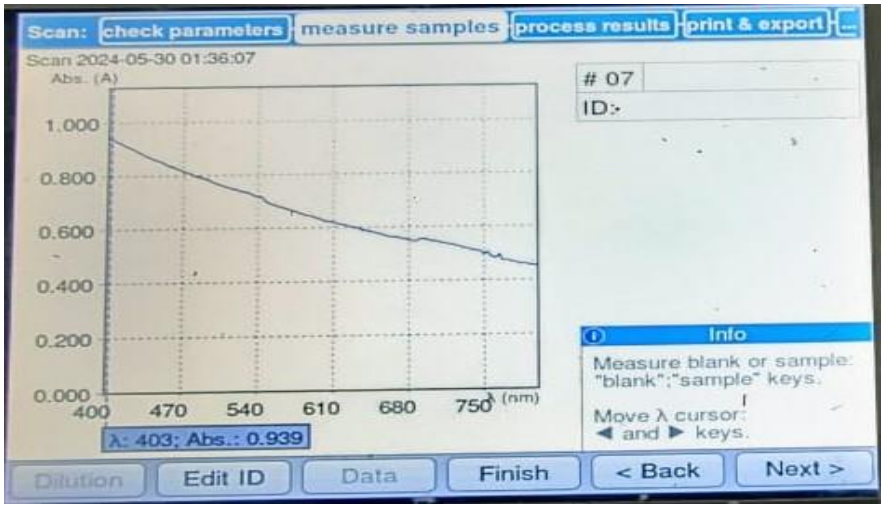

Fig. 21. UV-vis DRS for 50-Bi_4NbO_8Cl/g-C_3N_4

4.5 PHOTOCATALYTIC EXPERIMENT:

When catalysts are not present, MB degrades by 11% in 10 minutes. Thereafter, there is very little variation in photo-degradation, which reaches up to 16% over 60 minutes, suggesting that MB is reasonably stable when exposed to visible light. Within 60 minutes, only 35.44% and 44.07% of MB were degraded by BNOC and UGCN nanosheets, respectively. However, the combination of UGCN nanosheets with BNOC was found to significantly increase the photocatalytic efficiency for the breakdown of MB. In 60 minutes, the photocatalyst 50-BNOC/UGCN demonstrated the maximum degrading efficiency of 99.35% towards MB. To provide useful information on the reaction kinetics, the non-linear form of the pseudo first-order kinetics equation ($C = C_0 . e^{-kt}$) was fitted to the findings of MB degradation tests. The experimental data agreed well with the pseudo first-order kinetic equation, as shown by the R^2 values in Fig. 22(c). Additionally, it is noted that the 50-BNOC/UGCN nano-composite has the greatest apparent first-order rate constant (k) value (0.02711 min^{-1}), which is 1.3 and 2.7 times greater than that of the pristine BNOC (0.02109 min^{-1}) and UGCN nanosheets (0.0102 min^{-1}), respectively. The findings of some recent literature on the application of visible-light-assisted photocatalyst towards MB degradation have been presented in Table 3 to compare with the present study. It is evident that, when compared to the k values of the other investigations listed in Table 3, the k value of the 50-BNOC/UGCN nanocomposite was very comparable. Many dye degradation experiments have reported on the impact of pH. In the current instance, this parameter is likewise investigated, and Table 2 displays the findings. It was discovered that 81.08%, 97.96%, and 99.35%, of the dye (Methylene Blue, MB) could undergo degradation in 60 min in the presence of 50-BNOC/UGCN under the experimentally optimised conditions of MB (10ppm), catalyst amount= 1g/L, and pH of 4,7, and 9.2 respectively. After examining the impact of pH, it was found that, because the dye is cationic, its isoelectronic point (pHzpc) is equal to 9. Above 9, it is basic (anionic), and below 9, it is acidic (cationic) (Waghchaure et al., 2022).

Table: 2. Effect of pH on Methylene Blue (MB) degradation (MB = 10mg/L, Catalyst dose = 1g/L, Irradiation time = 60 minutes)

pH Value	% Degradation
4	81.08
7	97.96
9.2	99.35

Table: 3 Summary of the recent literature on photocatalytic MB degradation

Photocatalyst	Photocatalyst doses (g/l)	MB Concentration (mg/l)	Light Source	%Degradation / time (min)	Reference
WO_3/g-C_3N_4	0.5	50	300 W Xenon lamp	95%, 90 min	(Liu et al., 2017)
WO_3 ZnO@rGO	0.2	5	200 W tungsten filament lamp	94%, 90 min	(Chaudhary et al., 2020)
AgI/ZnO/WO_3	3.8	7	100 W tungsten filament lamp	85.2%, 48.5 min	(Ghattavi & Nezamzadeh-Ejhieh, 2021)
$CuFe_2O_4$/TiO_2	0.5	20	500 W Xenon lamp	83.7%, 3 hr	(Arifin et al., 2019)
BPN and ZnAl LDH	1	20	300 W xenon lamp	99%, 80 min	(Yang et al., 2021)
Ag@CdSe / Zeoilte	0.6	7.17	300 W tungsten halogen lamp	89.98%, 40 min	(Mosavi et al., 2021)
$Bi_{0.9}Gd_{0.07}La_{0.03}FeO_3$	0.45	20	120W	95%, 90 min	(Mani et al., 2022)
$Co_{0.5}Zn_{0.5}Mg_{0.5}Fe_{1.5}O_4$	0.05	10	300 W tungsten lamp	98.78%,60 min	(Chahar et al., 2023)
50Bi_4NbO_8Cl/ g-C_3N_4	1	10	20W LED lamp	99.35%, 60 min	This study

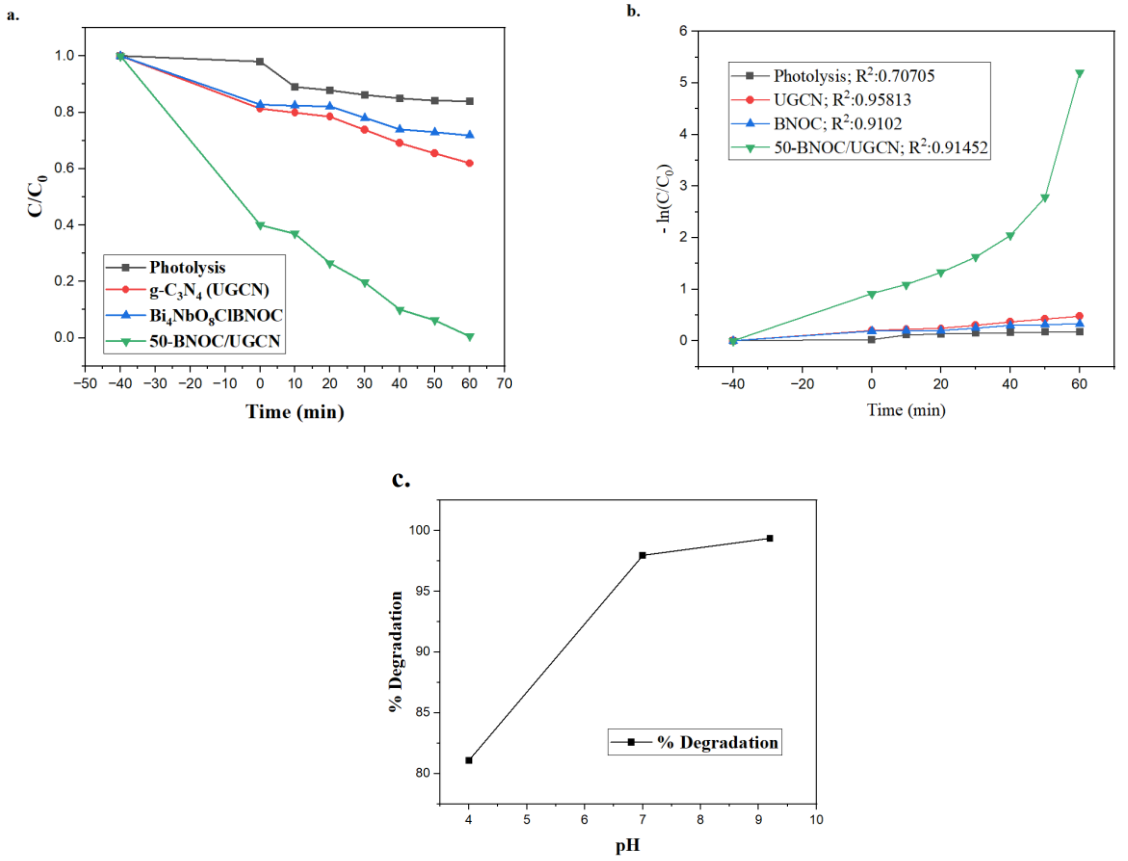

Fig 22. (a) Photocatalytic efficiency, (b) Pseudo first order reaction kinetics towards MB (10 mg/l) degradation, (c) Effect of pH.

4.6. RADICAL SCAVENGING EXPERIMENTS AND PHOTOCATALYTIC MECHANISM:

The main reactive species responsible for MB degradation were identified through a series of radical scavenging tests. The study's results are displayed in Fig.23. The degradation efficiency is significantly reduced upon the addition of BQ and EDTA2Na, suggesting that O_2 and h^+ are the primary reactive species in this investigation, respectively. The addition of IPA results in a minor reduction in degradation efficiency, demonstrating that OH has no effect on the 50-BNOC/UGCN nanocomposite's ability to degrade MB. Figure 24 presents a potential mechanism for the photocatalytic degradation of MB by the 50-BNOC/UGCN nano-composite, based on the band structure configuration of BNOC and UGCN, as well as the outcomes of radical scavenging studies. Both semiconductors generate charge carriers that are triggered by light when visible light exposure. The photogenerated electrons (e) in the CB of g-C_3N_4 will move to the CB of Bi_4NbO_8Cl because the CB of g-C_3N_4 (1.2 eV) is more negative

than the CB of Bi_4NbO_8Cl (0.54 eV). Since the VB of Bi_4NbO_8Cl (+2.07 eV) is more positive than the VB of g-C_3N_4 (+1.84 eV), the photogenerated holes (h^+) of Bi_4NbO_8Cl will migrate to the VB of g-C_3N_4. This will increase the electron and hole separation in g-C_3N_4 and Bi_4NbO_8Cl, leading to higher photocatalytic efficiency. Since the O_2/O_2 potential (0.33 eV vs. NHE) is greater than the ECB value (0.54 eV), the electrons in the Bi_4NbO_8Cl CB will therefore convert $O_2\backslash O_2$. MB will be weakened and mineralized by the potent oxidising agent known as the O_2 radical. However, because the E_{VB} value of g-C_3N_4 (+1.84 eV) is more negative than the potential of OH/H_2O (+2.68 eV vs. NHE) or OH/OH (+1.99 eV vs. NHE), the holes in the VB will not be able to oxidise H_2O or OH to ~OH. As a result, MB will be directly degraded and mineralized by the VB holes in g-C_3N_4. Thus, we may deduce that the 50-BNOC/UGCN nanocomposite employs a type-II heterojunction photocatalytic system for its electron-hole transport mechanism.

$$Bi_4NbO_8Cl + h\nu \longrightarrow e^-(Bi_4NbO_8Cl) + h^+(Bi_4NbO_8Cl) \quad \ldots(10)$$

$$g\text{-}C_3N_4 + h\nu \longrightarrow e^-(g\text{-}C_3N_4) + h^+(g\text{-}C_3N_4) \quad \ldots(11)$$

$$e^- g\text{-}C_3N_4 \longrightarrow e^-(Bi_4NbO_8Cl)\ \text{(Charge transfer)} \quad \ldots(12)$$

$$h^+(Bi_4NbO_8Cl) \longrightarrow h^+(g\text{-}C_3N_4)\ \text{(Charge transfer)} \quad \ldots(13)$$

$$e^-(Bi_4NbO_8Cl) + O_2 \longrightarrow \cdot O_2^- \quad \ldots(14)$$

$$\cdot O_2^- + MB \longrightarrow \text{By-products} + CO_2 + H_2O \quad \ldots(15)$$

$$h^+(g\text{-}C_3N_4) + MB \longrightarrow \text{By-products} + CO_2 + H_2O \quad \ldots(16)$$

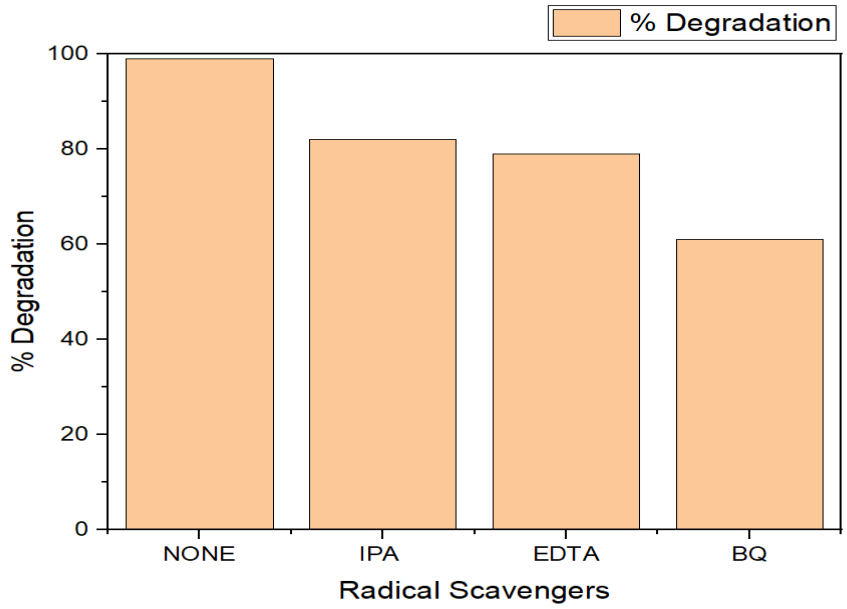

Fig 23: Photocatalytic degradation efficiency of 50-BNOC/UGCN nano-composites towards MB influenced by radical scavengers.

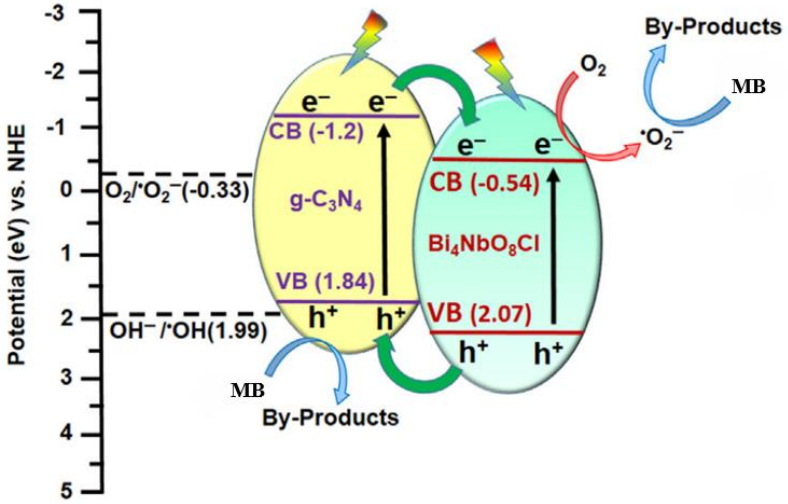

Fig:24: Schematic representation of the potential photocatalytic mechanism of the 50-BNOC/UGCN nano-composite during visible-light-assisted MB degradation.

Chapter:5

CONCLUSIONS:

A hydrothermal technique was used to successfully synthesize a novel Bi_4NbO_8Cl/g-C_3N_4 nano-composites, and reports of their photocatalytic efficiency towards MB degradation under visible light have been made. The results of different characterizations indicated that a strong contact was used to place the g-C_3N_4 nanosheets on the Bi_4NbO_8Cl surface. The optimised 50-BI_4NbO_8Cl/g-C_3N_4 nano-composite had the best MB degrading efficiency (99.35%) during 60 minutes of visible LED light irradiation. In comparison to pristine Bi_4NbO_8Cl and g-C_3N_4 nanosheets, the photocatalytic efficiency was 2.25 and 2.8 times higher, respectively. For the 50-Bi_4NbO_8Cl/g-C_3N_4 nano-composite, the apparent first order rate constant towards MB degradation was the highest (0.02711 min^{-1}). Due to its increased surface area, visible light absorption, and electron-hole pair separation, the 50-Bi_4NbO_8Cl/g-C_3N_4 nanocomposite exhibited higher photocatalytic efficiency when compared to pure Bi_4NbO_8Cl and g-C_3N_4. Moreover, the radical scavenging studies demonstrated that $^{\bullet}O_2^-$ & $OH^{\bullet}$ are the primary reactive species responsible for MB degradation over the 50-Bi_4NbO_8Cl/g-C_3N_4 nanocomposite. An energy band structure and radical scavenging tests have led to the suggestion of a Z-scheme heterojunction photocatalytic process. Consequently, the present study demonstrates the synthesis of a novel and efficient photocatalyst for the energy-efficient, low-cost treatment of dye pollutants with visible light assistance. This will stimulate the synthesis of more photocatalysts with similar properties for environmental remediation.

REFERENCES

Abid, M. F., Zablouk, M. A., & Abid-Alameer, A. M. (2012). Experimental study of dye removal from industrial wastewater by membrane technologies of reverse osmosis and nanofiltration. *Iranian Journal of Environmental Health Science and Engineering*, *9*(17). https://doi.org/10.1186/1735-2746-9-17

Aiman M.A Noman, Mohammed A. Alghobar, & Sidduraiah Suresha. (2021). Synthesis and activity evaluation of p-n CuO/CeO2-ZrO2 heterojunction photocatalyst for the removal of dye from industrial wastewater under Visible light irradiation. *Journal of Water and Environmental Nanotechnology*, 1–10.

Anjaneyulu, Y., Sreedhara Chary, N., & Samuel Suman Raj, D. (2005). Decolourization of Industrial Effluents – Available Methods and Emerging Technologies – A Review. *Reviews in Environmental Science and Bio/Technology*, *4*(4), 245–273. https://doi.org/10.1007/s11157-005-1246-z

Anwer, H., Mahmood, A., Lee, J., Kim, K.-H., Park, J.-W., & Yip, A. C. K. (2019). Photocatalysts for degradation of dyes in industrial effluents: Opportunities and challenges. *Nano Research*, *12*(5), 955–972. https://doi.org/10.1007/s12274-019-2287-0

Arifin, Md. N., Karim, K. Md. R., Abdullah, H., & Khan, M. R. (2019). Synthesis of Titania Doped Copper Ferrite Photocatalyst and Its Photoactivity towards Methylene Blue Degradation under Visible Light Irradiation. *Bulletin of Chemical Reaction Engineering & Catalysis*, *14*(1), 219–227. https://doi.org/10.9767/bcrec.14.1.3616.219-227

Arumugam, M., & Choi, M. Y. (2020). Recent progress on bismuth oxyiodide (BiOI) photocatalyst for environmental remediation. *Journal of Industrial and Engineering Chemistry*, *81*, 237–268. https://doi.org/10.1016/j.jiec.2019.09.013

Asadzadeh-Khaneghah, S., Habibi-Yangjeh, A., Seifzadeh, D., Chand, H., & Krishnan, V. (2021). Visible-light-activated g-C3N4 nanosheet/carbon dot/FeOCl nanocomposites: Photodegradation of dye pollutants and tetracycline hydrochloride. *Colloids and Surfaces A: Physicochemical and Engineering Aspects*, *617*, 126424. https://doi.org/10.1016/j.colsurfa.2021.126424

Ata, S., Shaheen, I., Qurat-ul-Ayne, Ghafoor, S., Sultan, M., Majid, F., Bibi, I., & Iqbal, M. (2018). Graphene and silver decorated ZnO composite synthesis, characterization and photocatalytic activity evaluation. *Diamond and Related Materials*, *90*, 26–31. https://doi.org/10.1016/j.diamond.2018.09.015

Avlonitis, G., Tsihrintzis, G., & Doukas, K. (2008). Treatment of textile wastewater by nanofiltration: Process performance and economic evaluation. *Desalination*, *226*(1–3), 212–221.

Avlonitis, S. A., Poulios, I., Sotiriou, D., Pappas, M., & Moutesidis, K. (2008). Simulated cotton dye effluents treatment and reuse by nanofiltration. *Desalination*, *221*(1–3), 259–267. https://doi.org/10.1016/j.desal.2007.01.082

Balasurya, S., Das, A., Alyousef, A. A., Alqasim, A., Almutairi, N., & Sudheer Khan, S. (2021). Facile synthesis of Bi2MoO6-Ag2MoO4 nanocomposite for the enhanced visible light photocatalytic removal of methylene blue and its antimicrobial application. *Journal of Molecular Liquids*, *337*, 116350. https://doi.org/10.1016/j.molliq.2021.116350

Beyene. (2014). The potential of dyes removal from textile wastewater by using different treatment technology, a review. *Int. J. Eng. Manag*, 347–353.

Cai, L., Zhou, Y., Ji, L., Guo, J., Liu, J., & Song, W. (2018). Synthesis of nano-Bi2MoO6/calcined mussel shell composite with enhanced visible light photocatalytic activity. *IOP Conference Series: Earth and Environmental Science*, *186*(2). https://doi.org/10.1088/1755-1315/186/2/012014

Carliell, C. M. B. C. A., Barclay, S. J., & Buckley, C. A. (1996). Buckley, C.A., 1996. Treatment of exhausted reactive dyebath effluent using anaerobic digestion: laboratory and full-scale trials. . *Water SA*, *22*, 225–233.

Chahar, D., Kumar, D., Thakur, P., & Thakur, A. (2023). Visible light induced photocatalytic degradation of methylene blue dye by using Mg doped Co-Zn nanoferrites. *Materials Research Bulletin*, *162*, 112205. https://doi.org/10.1016/j.materresbull.2023.112205

Chaudhary, K., Shaheen, N., Zulfiqar, S., Sarwar, M. I., Suleman, M., Agboola, P. O., Shakir, I., & Warsi, M. F. (2020). Binary WO3-ZnO nanostructures supported rGO ternary nanocomposite for visible light driven photocatalytic degradation of methylene blue. *Synthetic Metals*, *269*, 116526. https://doi.org/10.1016/j.synthmet.2020.116526

Chen, M., Shen, Y., Xu, L., Xiang, G., & Ni, Z. (2021). Highly efficient and rapid adsorption of methylene blue dye onto vinyl hybrid silica nano-cross-linked nanocomposite hydrogel. *Colloids and Surfaces A: Physicochemical and Engineering Aspects*, *613*. https://doi.org/10.1016/j.colsurfa.2020.126050

Chen, S., Hu, Y., Meng, S., & Fu, X. (2014). Study on the separation mechanisms of photogenerated electrons and holes for composite photocatalysts g-C3N4-WO3. *Applied Catalysis B: Environmental*, *150–151*, 564–573. https://doi.org/10.1016/j.apcatb.2013.12.053

Clark, M. (2011). *Handbook of textile and industrial dyeing*. Woodhead Publishing Limited. https://doi.org/10.1533/9780857094919

Crini. (2006). Non-conventional low-cost adsorbents for dye removal: A review. *Bioresource Technology*, *97*(9), 1061–1085. https://doi.org/10.1016/j.biortech.2005.05.001

Dalvand, A., Gholami, M., Joneidi, A., & Mahmoodi, N. M. (2011a). Dye Removal, Energy Consumption and Operating Cost of Electrocoagulation of Textile Wastewater as a Clean Process. *CLEAN – Soil, Air, Water*, *39*(7), 665–672. https://doi.org/10.1002/clen.201000233

Dalvand, A., Gholami, M., Joneidi, A., & Mahmoodi, N. M. (2011b). Dye Removal, Energy Consumption and Operating Cost of Electrocoagulation of Textile Wastewater as a Clean Process. *CLEAN – Soil, Air, Water*, *39*(7), 665–672. https://doi.org/10.1002/clen.201000233

Daneshvar, N., Ayazloo, M., Khataee, A. R., & Pourhassan, M. (2007). Biological decolorization of dye solution containing Malachite Green by microalgae Cosmarium sp. *Bioresource Technology*, *98*(6), 1176–1182. https://doi.org/10.1016/j.biortech.2006.05.025

Deb, B., & Ghosh, A. (2011). Silver Ion Dynamics in Ag_2S-Doped Silver Molybdate–Glass Nanocomposites: Correlation of Conductivity and Scaling with Structure. *The Journal of Physical Chemistry C*, *115*(29), 14141–14147. https://doi.org/10.1021/jp204474n

Dias, J. M., Alvim-Ferraz, M. C. M., Almeida, M. F., Rivera-Utrilla, J., & Sánchez-Polo, M. (2007). Waste materials for activated carbon preparation and its use in aqueous-phase treatment: A review.

Journal of Environmental Management, *85*(4), 833–846. https://doi.org/10.1016/j.jenvman.2007.07.031

Ding, J., Xu, W., Wan, H., Yuan, D., Chen, C., Wang, L., Guan, G., & Dai, W.-L. (2018). Nitrogen vacancy engineered graphitic C3N4-based polymers for photocatalytic oxidation of aromatic alcohols to aldehydes. *Applied Catalysis B: Environmental*, *221*, 626–634. https://doi.org/10.1016/j.apcatb.2017.09.048

Dutta, S., Bhattacharyya, A., Ganguly, A., Gupta, S., & Basu, S. (2011). Application of Response Surface Methodology for preparation of low-cost adsorbent from citrus fruit peel and for removal of Methylene Blue. *Desalination*, *275*(1–3), 26–36. https://doi.org/10.1016/j.desal.2011.02.057

El Qada, E. N., Allen, S. J., & Walker, G. M. (2008). Adsorption of basic dyes from aqueous solution onto activated carbons. *Chemical Engineering Journal*, *135*(3), 174–184. https://doi.org/10.1016/j.cej.2007.02.023

El-Katori, E. E., Ahmed, M. A., El-Bindary, A. A., & Oraby, A. M. (2020). Impact of CdS/SnO2 heterostructured nanoparticle as visible light active photocatalyst for the removal methylene blue dye. *Journal of Photochemistry and Photobiology A: Chemistry*, *392*, 112403. https://doi.org/10.1016/j.jphotochem.2020.112403

Epling, G. A., & Lin, C. (2002). Photoassisted bleaching of dyes utilizing TiO2 and visible light. *Chemosphere*, *46*(4), 561–570. https://doi.org/10.1016/S0045-6535(01)00173-4

Ferreira, W. H., Silva, L. G. A., Pereira, B. C. S., Gouvêa, R. F., & Andrade, C. T. (2020). Adsorption and visible-light photocatalytic performance of a graphene derivative for methylene blue degradation. *Environmental Nanotechnology, Monitoring & Management*, *14*, 100373. https://doi.org/10.1016/j.enmm.2020.100373

Fujito, H., Kunioku, H., Kato, D., Suzuki, H., Higashi, M., Kageyama, H., & Abe, R. (2016). Layered Perovskite Oxychloride Bi $_4$ NbO $_8$ Cl: A Stable Visible Light Responsive Photocatalyst for Water Splitting. *Journal of the American Chemical Society*, *138*(7), 2082–2085. https://doi.org/10.1021/jacs.5b11191

Gao, L., Du, J., & Ma, T. (2017a). Cysteine-assisted synthesis of CuS-TiO 2 composites with enhanced photocatalytic activity. *Ceramics International*, *43*(12), 9559–9563. https://doi.org/10.1016/j.ceramint.2017.04.093

Gao, L., Du, J., & Ma, T. (2017b). Cysteine-assisted synthesis of CuS-TiO 2 composites with enhanced photocatalytic activity. *Ceramics International*, *43*(12), 9559–9563. https://doi.org/10.1016/j.ceramint.2017.04.093

Ghattavi, S., & Nezamzadeh-Ejhieh, A. (2021). A double-Z-scheme ZnO/AgI/WO3 photocatalyst with high visible light activity: Experimental design and mechanism pathway in the degradation of methylene blue. *Journal of Molecular Liquids*, *322*, 114563. https://doi.org/10.1016/j.molliq.2020.114563

Ghosh, U., & Pal, A. (2020a). Fabrication of a novel Bi2O3 nanoparticle impregnated nitrogen vacant 2D g-C3N4 nanosheet Z scheme photocatalyst for improved degradation of methylene blue dye under LED light illumination. *Applied Surface Science*, *507*, 144965. https://doi.org/10.1016/j.apsusc.2019.144965

Ghosh, U., & Pal, A. (2020b). Fabrication of a novel Bi2O3 nanoparticle impregnated nitrogen vacant 2D g-C3N4 nanosheet Z scheme photocatalyst for improved degradation of methylene blue dye under LED light illumination. *Applied Surface Science*, *507*, 144965. https://doi.org/10.1016/j.apsusc.2019.144965

Goud, B. S., Koyyada, G., Jung, J. H., Reddy, G. R., Shim, J., Nam, N. D., & Vattikuti, S. V. P. (2020). Surface oxygen vacancy facilitated Z-scheme MoS2/Bi2O3 heterojunction for enhanced visible-light driven photocatalysis-pollutant degradation and hydrogen production. *International Journal of Hydrogen Energy*, *45*(38), 18961–18975. https://doi.org/10.1016/j.ijhydene.2020.05.073

Gouveia, A. F., Sczancoski, J. C., Ferrer, M. M., Lima, A. S., Santos, M. R. M. C., Li, M. S., Santos, R. S., Longo, E., & Cavalcante, L. S. (2014). Experimental and Theoretical Investigations of Electronic Structure and Photoluminescence Properties of β-Ag_2MoO_4 Microcrystals. *Inorganic Chemistry*, *53*(11), 5589–5599. https://doi.org/10.1021/ic500335x

Gozálvez-Zafrilla, J. M., Sanz-Escribano, D., Lora-García, J., & León Hidalgo, M. C. (2008). Nanofiltration of secondary effluent for wastewater reuse in the textile industry. *Desalination*, *222*(1–3), 272–279. https://doi.org/10.1016/j.desal.2007.01.173

Guo, F., Shi, W., Lin, X., & Che, G. (2014). Hydrothermal synthesis of graphitic carbon nitride-BiVO4 composites with enhanced visible light photocatalytic activities and the mechanism study. *Journal of Physics and Chemistry of Solids*, *75*(11), 1217–1222. https://doi.org/10.1016/j.jpcs.2014.05.011

Hameed, B. H., Ahmad, A. L., & Latiff, K. N. A. (2007). Adsorption of basic dye (methylene blue) onto activated carbon prepared from rattan sawdust. *Dyes and Pigments*, *75*(1), 143–149. https://doi.org/10.1016/j.dyepig.2006.05.039

Hassaan, M. A., El Nemr, A., & Madkour, F. F. (2017). Testing the advanced oxidation processes on the degradation of Direct Blue 86 dye in wastewater. *Egyptian Journal of Aquatic Research*, *43*(1), 11–19. https://doi.org/10.1016/j.ejar.2016.09.006

Hassani, A. H., Mirzayee, R., Nasseri, S., Borghei, M., Gholami, M., & Torabifar, B. (2008). Nanofiltration process on dye removal from simulated textile wastewater. *Int. J. Environ. Sci. Tech*, *5*(3), 401–408.

He, Y., Zhang, L., Teng, B., & Fan, M. (2015). New Application of Z-Scheme Ag_3PO_4/g-C_3N_4 Composite in Converting CO_2 to Fuel. *Environmental Science & Technology*, *49*(1), 649–656. https://doi.org/10.1021/es5046309

Hong, Y., Jiang, Y., Li, C., Fan, W., Yan, X., Yan, M., & Shi, W. (2016). In-situ synthesis of direct solid-state Z-scheme V2O5/g-C3N4 heterojunctions with enhanced visible light efficiency in photocatalytic degradation of pollutants. *Applied Catalysis B: Environmental*, *180*, 663–673. https://doi.org/10.1016/j.apcatb.2015.06.057

Huang, H., Chen, F., Reshak, A. H., Auluck, S., & Zhang, Y. (2018). Insight into crystal-structure dependent charge separation and photo-redox catalysis: A combined experimental and theoretical study on Bi(IO3)3 and BiOIO3. *Applied Surface Science*, *458*, 129–138. https://doi.org/10.1016/j.apsusc.2018.07.054

Huang, Y., Li, H., Balogun, M.-S., Liu, W., Tong, Y., Lu, X., & Ji, H. (2014). Oxygen Vacancy Induced Bismuth Oxyiodide with Remarkably Increased Visible-Light Absorption and Superior

Photocatalytic Performance. *ACS Applied Materials & Interfaces*, *6*(24), 22920–22927. https://doi.org/10.1021/am507641k

Huang, Z., Jia, S., Wei, J., & Shao, Z. (2021a). A visible light active, carbon–nitrogen–sulfur co-doped TiO_2/g-C_3N_4 Z-scheme heterojunction as an effective photocatalyst to remove dye pollutants. *RSC Advances*, *11*(27), 16747–16754. https://doi.org/10.1039/D1RA01890F

Huang, Z., Jia, S., Wei, J., & Shao, Z. (2021b). A visible light active, carbon-nitrogen-sulfur co-doped TiO2/g-C3N4Z-scheme heterojunction as an effective photocatalyst to remove dye pollutants. *RSC Advances*, *11*(27), 16747–16754.

Iqbal, M., Bhatti, H. N., Younis, S., Rehmat, S., Alwadai, N., Almuqrin, A. H., & Iqbal, M. (2021). Graphene oxide nanocomposite with CuSe and photocatalytic removal of methyl green dye under visible light irradiation. *Diamond and Related Materials*, *113*, 108254. https://doi.org/10.1016/j.diamond.2021.108254

Jana, A., & Gregory, D. H. (2020). Microwave-Assisted Synthesis of ZnO–rGO Core–Shell Nanorod Hybrids with Photo- and Electro-Catalytic Activity. *Chemistry – A European Journal*, *26*(29), 6703–6714. https://doi.org/10.1002/chem.202000535

Katheresan, V., Kansedo, J., & Lau, S. Y. (2018). Efficiency of various recent wastewater dye removal methods: A review. In *Journal of Environmental Chemical Engineering* (Vol. 6, Issue 4, pp. 4676–4697). Elsevier Ltd. https://doi.org/10.1016/j.jece.2018.06.060

Khan, M. E., Khan, M. M., & Cho, M. H. (2017). Ce3+-ion, Surface Oxygen Vacancy, and Visible Light-induced Photocatalytic Dye Degradation and Photocapacitive Performance of CeO2-Graphene Nanostructures. *Scientific Reports*, *7*(1), 5928. https://doi.org/10.1038/s41598-017-06139-6

Kumar, S., T, S., Kumar, B., Baruah, A., & Shanker, V. (2013). Synthesis of Magnetically Separable and Recyclable g-C_3N_4–Fe_3O_4 Hybrid Nanocomposites with Enhanced Photocatalytic Performance under Visible-Light Irradiation. *The Journal of Physical Chemistry C*, *117*(49), 26135–26143. https://doi.org/10.1021/jp409651g

Lei, Y., Ding, J., Yu, P., He, G., Chen, Y., & Chen, H. (2020). Low-temperature preparation of magnetically separable Fe3O4@ZnO-RGO for high-performance removal of methylene blue in visible light. *Journal of Alloys and Compounds*, *821*, 153366. https://doi.org/10.1016/j.jallcom.2019.153366

Li, H., Zhou, Y., Tu, W., Ye, J., & Zou, Z. (2015). State-of-the-Art Progress in Diverse Heterostructured Photocatalysts toward Promoting Photocatalytic Performance. *Advanced Functional Materials*, *25*(7), 998–1013. https://doi.org/10.1002/adfm.201401636

Li, X., Ju, Z., Li, F., Huang, Y., Xie, Y., Fu, Z., Knize, R. J., & Lu, Y. (2014). Visible light responsive $Bi_7Fe_3Ti_3O_{21}$ nanoshelf photocatalysts with ferroelectricity and ferromagnetism. *Journal of Materials Chemistry A*, *2*(33), 13366. https://doi.org/10.1039/C4TA01799D

Liang, M., Yang, Z., Mei, Y., Zhou, H., & Yang, S. (2018). Dye-Sensitized-Assisted, Enhanced Photocatalytic Activity of TiO_2/$Bi_4V_2O_{11}$. *Nano*, *13*(03), 1850028. https://doi.org/10.1142/S1793292018500285

Lin, X., Huang, T., Huang, F., Wang, W., & Shi, J. (2007a). Photocatalytic Activity of a Bi-Based Oxychloride Bi_3O_4Cl. *ChemInform*, *38*(18). https://doi.org/10.1002/chin.200718020

Lin, X., Huang, T., Huang, F., Wang, W., & Shi, J. (2007b). Photocatalytic activity of a Bi-based oxychloride Bi4NbO8Cl. *Journal of Materials Chemistry*, *17*(20), 2145. https://doi.org/10.1039/b615903f

Liu, X., Jin, A., Jia, Y., Xia, T., Deng, C., Zhu, M., Chen, C., & Chen, X. (2017). Synergy of adsorption and visible-light photocatalytic degradation of methylene blue by a bifunctional Z-scheme heterojunction of WO3/g-C3N4. *Applied Surface Science*, *405*, 359–371. https://doi.org/10.1016/j.apsusc.2017.02.025

Ma, Y., Chen, Y., Feng, Z., Zeng, L., Chen, Q., Jin, R., Lu, Y., Huang, Y., Wu, Y., & He, Y. (2017). Preparation, characterization of Bi 3 O 4 Cl/g-C 3 N 4 composite and its photocatalytic activity in dye degradation. *Journal of Water Process Engineering*, *18*, 65–72. https://doi.org/10.1016/j.jwpe.2017.06.002

Majumdar, A., Ghosh, U., & Pal, A. (2021). Novel 2D/2D g-C3N4/Bi4NbO8Cl nano-composite for enhanced photocatalytic degradation of oxytetracycline under visible LED light irradiation. *Journal of Colloid and Interface Science*, *584*, 320–331. https://doi.org/10.1016/j.jcis.2020.09.101

Majumdar, A., & Pal, A. (2020). Recent advancements in visible-light-assisted photocatalytic removal of aqueous pharmaceutical pollutants. In *Clean Technologies and Environmental Policy* (Vol. 22, Issue 1, pp. 11–42). Springer Science and Business Media Deutschland GmbH. https://doi.org/10.1007/s10098-019-01766-1

Mani, A. D., Li, J., Wang, Z., Zhou, J., Xiang, H., Zhao, J., Deng, L., Yang, H., & Yao, L. (2022). Coupling of piezocatalysis and photocatalysis for efficient degradation of methylene blue by Bi0.9Gd0.07La0.03FeO3 nanotubes. *Journal of Advanced Ceramics*, *11*(7), 1069–1081. https://doi.org/10.1007/s40145-022-0590-6

Mao, W., Zhang, L., Wang, T., Bai, Y., & Guan, Y. (2021). Fabrication of highly efficient Bi2WO6/CuS composite for visible-light photocatalytic removal of organic pollutants and Cr(VI) from wastewater. *Frontiers of Environmental Science & Engineering*, *15*(4), 52. https://doi.org/10.1007/s11783-020-1344-8

Meng, Z., & Juan, Z. (n.d.). *Wastewater treatment by photocatalytic oxidation of Nano-ZnO*.

Mohamad Idris, N. H., Rajakumar, J., Cheong, K. Y., Kennedy, B. J., Ohno, T., Yamakata, A., & Lee, H. L. (2021a). Titanium Dioxide/Polyvinyl Alcohol/Cork Nanocomposite: A Floating Photocatalyst for the Degradation of Methylene Blue under Irradiation of a Visible Light Source. *ACS Omega*, *6*(22), 14493–14503. https://doi.org/10.1021/acsomega.1c01458

Mohamad Idris, N. H., Rajakumar, J., Cheong, K. Y., Kennedy, B. J., Ohno, T., Yamakata, A., & Lee, H. L. (2021b). Titanium Dioxide/Polyvinyl Alcohol/Cork Nanocomposite: A Floating Photocatalyst for the Degradation of Methylene Blue under Irradiation of a Visible Light Source. *ACS Omega*, *6*(22), 14493–14503. https://doi.org/10.1021/acsomega.1c01458

Mohamed, R. M., McKinney, D. L., & Sigmund, W. M. (2012). Enhanced nanocatalysts. In *Materials Science and Engineering R: Reports* (Vol. 73, Issue 1, pp. 1–13). https://doi.org/10.1016/j.mser.2011.09.001

Mohan, D., Tiwari, R. K., & Sillanpää, M. (2002). Adsorption of crystal violet and basic fuchsine from aqueous solution onto fly ash. *Journal of Hazardous Materials*, *92*(1–3), 147–156.

Mokif, L. A. (2019). Removal Methods of Synthetic Dyes from Industrial Wastewater: A review. *Mesopo. Environ. J*, *5*(1), 23–40. https://doi.org/10.31759/mej.2019.5.1.0040

Mosavi, S. A., Ghadi, A., Gharbani, P., & Mehrizad, A. (2021). Photocatalytic removal of Methylene Blue using Ag@CdSe/Zeoilte nanocomposite under visible light irradiation by Response Surface Methodology. *Materials Chemistry and Physics*, *267*, 124696. https://doi.org/10.1016/j.matchemphys.2021.124696

Natarajan, S., Bajaj, H. C., & Tayade, R. J. (2018a). Recent advances based on the synergetic effect of adsorption for removal of dyes from waste water using photocatalytic process. *Journal of Environmental Sciences*, *65*, 201–222. https://doi.org/10.1016/j.jes.2017.03.011

Natarajan, S., Bajaj, H. C., & Tayade, R. J. (2018b). Recent advances based on the synergetic effect of adsorption for removal of dyes from waste water using photocatalytic process. *Journal of Environmental Sciences*, *65*, 201–222. https://doi.org/10.1016/j.jes.2017.03.011

Ni, G., Li, Y., Chen, H., Wang, Z., Qin, X., Zhang, X., Huang, B., Li, F., & Liu, H. (2019). The Sol–gel method synthesis of Bi 4 NbO 8 Cl with (001) facets exposed for high visible-light activity. *Journal of Materials Science: Materials in Electronics*. https://doi.org/10.1007/s10854-019-01112-7

Niu, P., Qiao, M., Li, Y., Huang, L., & Zhai, T. (2018). Distinctive defects engineering in graphitic carbon nitride for greatly extended visible light photocatalytic hydrogen evolution. *Nano Energy*, *44*, 73–81. https://doi.org/10.1016/j.nanoen.2017.11.059

Ogawa, K., Nakada, A., Suzuki, H., Tomita, O., Higashi, M., Saeki, A., Kageyama, H., & Abe, R. (2019a). Flux Synthesis of Layered Oxyhalide Bi_4NbO_8Cl Photocatalyst for Efficient *Z* -Scheme Water Splitting Under Visible Light. *ACS Applied Materials & Interfaces*, *11*(6), 5642–5650. https://doi.org/10.1021/acsami.8b06411

Ogawa, K., Nakada, A., Suzuki, H., Tomita, O., Higashi, M., Saeki, A., Kageyama, H., & Abe, R. (2019b). Flux Synthesis of Layered Oxyhalide Bi_4NbO_8Cl Photocatalyst for Efficient *Z* -Scheme Water Splitting Under Visible Light. *ACS Applied Materials & Interfaces*, *11*(6), 5642–5650. https://doi.org/10.1021/acsami.8b06411

Oladoye, P. O., Ajiboye, T. O., Omotola, E. O., & Oyewola, O. J. (2022). Methylene blue dye: Toxicity and potential elimination technology from wastewater. In *Results in Engineering* (Vol. 16). Elsevier B.V. https://doi.org/10.1016/j.rineng.2022.100678

Ou, H., Lin, L., Zheng, Y., Yang, P., Fang, Y., & Wang, X. (2017). Tri- *s* -triazine-Based Crystalline Carbon Nitride Nanosheets for an Improved Hydrogen Evolution. *Advanced Materials*, *29*(22). https://doi.org/10.1002/adma.201700008

Pan, H., Feng, J., He, G.-X., Cerniglia, C. E., & Chen, H. (2012). Evaluation of impact of exposure of Sudan azo dyes and their metabolites on human intestinal bacteria. *Anaerobe*, *18*(4), 445–453. https://doi.org/10.1016/j.anaerobe.2012.05.002

Panneri, S., Ganguly, P., Mohan, M., Nair, B. N., Mohamed, A. A. P., Warrier, K. G., & Hareesh, U. S. (2017). Photoregenerable, Bifunctional Granules of Carbon-Doped g-C_3N_4 as Adsorptive Photocatalyst for the Efficient Removal of Tetracycline Antibiotic. *ACS Sustainable Chemistry & Engineering*, *5*(2), 1610–1618. https://doi.org/10.1021/acssuschemeng.6b02383

Paquin, F., Rivnay, J., Salleo, A., Stingelin, N., & Silva-Acuña, C. (2015). Multi-phase microstructures drive exciton dissociation in neat semicrystalline polymeric semiconductors. *Journal of Materials Chemistry C*, *3*(41), 10715–10722. https://doi.org/10.1039/C5TC02043C

Pelaez, M., Nolan, N. T., Pillai, S. C., Seery, M. K., Falaras, P., Kontos, A. G., Dunlop, P. S. M., Hamilton, J. W. J., Byrne, J. A., O'Shea, K., Entezari, M. H., & Dionysiou, D. D. (2012). A review on the visible light active titanium dioxide photocatalysts for environmental applications. *Applied Catalysis B: Environmental*, *125*, 331–349. https://doi.org/10.1016/j.apcatb.2012.05.036

Prabakaran, E., & Pillay, K. (2019). Synthesis of N-doped ZnO nanoparticles with cabbage morphology as a catalyst for the efficient photocatalytic degradation of methylene blue under UV and visible light. *RSC Advances*, *9*(13), 7509–7535.

PRUDEN, A. (1983). Photoassisted heterogeneous catalysis: The degradation of trichloroethylene in water. *Journal of Catalysis*, *82*(2), 404–417. https://doi.org/10.1016/0021-9517(83)90207-5

Sá, J., Fernández-García, M., & Anderson, J. A. (2008). Photoformed electron transfer from TiO2 to metal clusters. *Catalysis Communications*, *9*(10), 1991–1995. https://doi.org/10.1016/j.catcom.2008.03.041

Sanakousar, F. M., Vidyasagar, C. C., Jiménez-Pérez, V. M., & Prakash, K. (2022). Recent progress on visible-light-driven metal and non-metal doped ZnO nanostructures for photocatalytic degradation of organic pollutants. *Materials Science in Semiconductor Processing*, *140*, 106390. https://doi.org/10.1016/j.mssp.2021.106390

Sharma, J., Sharma, S., & Soni, V. (2021). Classification and impact of synthetic textile dyes on Aquatic Flora: A review. *Regional Studies in Marine Science*, *45*, 101802. https://doi.org/10.1016/j.rsma.2021.101802

Shen, S., Guo, L., Chen, X., Ren, F., Kronawitter, C. X., & Mao, S. S. (2010). Effect of Noble Metal in CdS/M/TiO $_2$ for Photocatalytic Degradation of Methylene Blue under Visible Light. *International Journal of Green Nanotechnology: Materials Science & Engineering*, *1*(2), M94–M104. https://doi.org/10.1080/19430841003684823

Shi, L., Liang, L., Ma, J., Meng, Y., Zhong, S., Wang, F., & Sun, J. (2014). Highly efficient visible light-driven Ag/AgBr/ZnO composite photocatalyst for degrading Rhodamine B. *Ceramics International*, *40*(2), 3495–3502. https://doi.org/10.1016/j.ceramint.2013.09.080

Shinde, S. S., Bhosale, C. H., & Rajpure, K. Y. (2012). Photocatalytic degradation of toluene using sprayed N-doped ZnO thin films in aqueous suspension. *Journal of Photochemistry and Photobiology B: Biology*, *113*, 70–77. https://doi.org/10.1016/j.jphotobiol.2012.05.008

Stephenson @, R. J., & Dufft, S. J. B. (1996). COAGULATION AND PRECIPITATION OF A MECHANICAL PULPING EFFLUENT-I. REMOVAL OF CARBON, COLOUR AND TURBIDITY. In *War. ICes* (Vol. 30, Issue 95).

Sun, Y., Wang, W., Zhang, L., & Sun, S. (2013). The photocatalysis of Bi2MoO6 under the irradiation of blue LED. *Materials Research Bulletin*, *48*(10), 4357–4361. https://doi.org/10.1016/j.materresbull.2013.07.015

Surolia, P. K., Tayade, R. J., & Jasra, R. V. (2010). Photocatalytic Degradation of Nitrobenzene in an Aqueous System by Transition-Metal-Exchanged ETS-10 Zeolites. *Industrial & Engineering Chemistry Research*, *49*(8), 3961–3966. https://doi.org/10.1021/ie901603k

Thabede, P. M., Shooto, N. D., & Naidoo, E. B. (2020). Removal of methylene blue dye and lead ions from aqueous solution using activated carbon from black cumin seeds. *South African Journal of Chemical Engineering*, *33*, 39–50. https://doi.org/10.1016/j.sajce.2020.04.002

Viswanathan, B. (2017). Photocatalytic Degradation of Dyes: An Overview. *Current Catalysis*, *7*(2), 99–121. https://doi.org/10.2174/2211544707666171219161846

Waghchaure, R. H., Adole, V. A., & Jagdale, B. S. (2022). Photocatalytic degradation of methylene blue, rhodamine B, methyl orange and Eriochrome black T dyes by modified ZnO nanocatalysts: A concise review. *Inorganic Chemistry Communications*, *143*, 109764. https://doi.org/10.1016/j.inoche.2022.109764

Wang, M., Tan, G., Zhang, D., Li, B., Lv, L., Wang, Y., Ren, H., Zhang, X., Xia, A., & Liu, Y. (2019). Defect-mediated Z-scheme BiO2-x/Bi2O2.75 photocatalyst for full spectrum solar-driven organic dyes degradation. *Applied Catalysis B: Environmental*, *254*, 98–112. https://doi.org/10.1016/j.apcatb.2019.04.044

Wu, D., Wang, B., Wang, W., An, T., Li, G., Ng, T. W., Yip, H. Y., Xiong, C., Lee, H. K., & Wong, P. K. (2015). Visible-light-driven BiOBr nanosheets for highly facet-dependent photocatalytic inactivation of Escherichia coli. *Journal of Materials Chemistry A*, *3*(29), 15148–15155. https://doi.org/10.1039/C5TA02757H

Xing, C., Wu, Z., Jiang, D., & Chen, M. (2014). Hydrothermal synthesis of In2S3/g-C3N4 heterojunctions with enhanced photocatalytic activity. *Journal of Colloid and Interface Science*, *433*, 9–15. https://doi.org/10.1016/j.jcis.2014.07.015

Xu, Q., Zhang, L., Yu, J., Wageh, S., Al-Ghamdi, A. A., & Jaroniec, M. (2018). Direct Z-scheme photocatalysts: Principles, synthesis, and applications. *Materials Today*, *21*(10), 1042–1063. https://doi.org/10.1016/j.mattod.2018.04.008

Xu, Y., Lin, D., Liu, X., Luo, Y., Xue, H., Huang, B., Chen, Q., & Qian, Q. (2018). Electrospun BiOCl/$Bi_2Ti_2O_7$ Nanorod Heterostructures with Enhanced Solar Light Efficiency in the Photocatalytic Degradation of Tetracycline Hydrochloride. *ChemCatChem*, *10*(11), 2496–2504. https://doi.org/10.1002/cctc.201800100

Xue, J., Ma, S., Zhou, Y., Zhang, Z., & He, M. (2015). Facile Photochemical Synthesis of Au/Pt/g-C_3N_4 with Plasmon-Enhanced Photocatalytic Activity for Antibiotic Degradation. *ACS Applied Materials & Interfaces*, *7*(18), 9630–9637. https://doi.org/10.1021/acsami.5b01212

Yan, C., & Liu, L. (2020). Sn-doped V2O5 nanoparticles as catalyst for fast removal of ammonia in air via PEC and PEC-MFC. *Chemical Engineering Journal*, *392*, 123738. https://doi.org/10.1016/j.cej.2019.123738

Yang, J., Jing, R., Wang, P., Liang, D., Huang, H., Xia, C., Zhang, Q., Liu, A., Meng, Z., & Liu, Y. (2021). Black phosphorus nanosheets and ZnAl-LDH nanocomposite as environmental-friendly photocatalysts for the degradation of Methylene blue under visible light irradiation. *Applied Clay Science*, *200*, 105902. https://doi.org/10.1016/j.clay.2020.105902

Yu, Y., Gu, Y., Zheng, W., Ding, Y., & Cao, Y. (2015). New Type Photocatalyst $PbBiO_2Cl$: Materials Design and Experimental Validation. *The Journal of Physical Chemistry C*, *119*(50), 28190–28193. https://doi.org/10.1021/acs.jpcc.5b09281

Zhang, D. (2012a). Visible light-induced photocatalysis through surface plasmon excitation of platinum-metallized titania for photocatalytic bleaching of rhodamine B. *Monatshefte Für Chemie - Chemical Monthly*, *143*(5), 729–738. https://doi.org/10.1007/s00706-011-0631-2

Zhang, D. (2012b). Visible light-induced photocatalysis through surface plasmon excitation of platinum-metallized titania for photocatalytic bleaching of rhodamine B. *Monatshefte Für Chemie - Chemical Monthly*, *143*(5), 729–738. https://doi.org/10.1007/s00706-011-0631-2

Zhang, J., Hu, Y., Jiang, X., Chen, S., Meng, S., & Fu, X. (2014). Design of a direct Z-scheme photocatalyst: Preparation and characterization of Bi2O3/g-C3N4 with high visible light activity. *Journal of Hazardous Materials*, *280*, 713–722. https://doi.org/10.1016/j.jhazmat.2014.08.055

Zhang, J., Lee, K. H., Cui, L., & Jeong, T. seop. (2009). Degradation of methylene blue in aqueous solution by ozone-based processes. *Journal of Industrial and Engineering Chemistry*, *15*(2), 185–189. https://doi.org/10.1016/j.jiec.2008.09.014

Zhang, W., Liu, X., Dong, X., Dong, F., & Zhang, Y. (2017). Facile synthesis of Bi12O17Br2 and Bi4O5Br2 nanosheets: In situ DRIFTS investigation of photocatalytic NO oxidation conversion pathway. *Chinese Journal of Catalysis*, *38*(12), 2030–2038. https://doi.org/10.1016/S1872-2067(17)62941-3

Zhang, X., Jia, X., Duan, P., Xia, R., Zhang, N., Cheng, B., Wang, Z., & Zhang, Y. (2021). V2O5/P-g-C3N4 Z-scheme enhanced heterogeneous photocatalytic removal of methyl orange from water under visible light irradiation. *Colloids and Surfaces A: Physicochemical and Engineering Aspects*, *608*, 125580. https://doi.org/10.1016/j.colsurfa.2020.125580

Zhang, X., Xie, X., Wang, H., Zhang, J., Pan, B., & Xie, Y. (2013). Enhanced Photoresponsive Ultrathin Graphitic-Phase C_3N_4 Nanosheets for Bioimaging. *Journal of the American Chemical Society*, *135*(1), 18–21. https://doi.org/10.1021/ja308249k

Zhang, Y., Chen, Z., Shi, Z., Lu, T., Chen, D., Wang, Q., & Zhan, Z. (2021). A direct Z-scheme BiOBr/TzDa COF heterojunction photocatalyst with enhanced performance on visible-light driven removal of organic dye and Cr(VI). *Separation and Purification Technology*, *275*, 119216. https://doi.org/10.1016/j.seppur.2021.119216

Zhang, Z., Zhao, C., Lin, S., Li, H., Feng, Y., & Gao, X. (2021). Oxygen vacancy modified Bi2MoO6/WO3 electrode with enhanced photoelectrocatalytic degradation activity toward RhB. *Fuel*, *285*, 119171. https://doi.org/10.1016/j.fuel.2020.119171

Zhao, X., Li, M., & Lou, X. (2014). Sol-gel assisted hydrothermal synthesis of ZnO microstructures: Morphology control and photocatalytic activity. *Advanced Powder Technology*, *25*(1), 372–378. https://doi.org/10.1016/j.apt.2013.06.004

Zollinger H. (1987). *Color Chemistry-Synthesis, Properties and Application of Organic Dyes and Pigments* (3rd ed.).